Simple octagonal and dodecagonal quasicrystals

Joshua E. S. Socolar
Department of Physics, Harvard University, Cambridge, Massachusetts 02138
(Received 27 December 1988)

Penrose tilings have become the canonical model for quasicrystal structure, primarily because of their simplicity in comparison with other decagonally symmetric quasiperiodic tilings of the plane. Four remarkable properties of the Penrose tilings have been exploited in the analysis of the physical issues: (1) the class of Penrose tilings is invariant under *deflation* (a type of self-similarity transformation); (2) the class contains all tilings consistent with a set of *matching rules* governing the orientations of neighboring tiles; (3) a certain decoration of the tiles produces grids of quasiperiodically spaced Ammann lines; and (4) the tile vertices can be obtained by projection of a subset of hypercubic lattice points. Each of the first three properties can be explicitly displayed by means of a *simple* decoration of the tiles, a decoration in which all the marked tiles of a given shape are related by the operations in the orientational symmetry group of the tiling. In this paper, analogues of the Penrose tilings are presented for the cases of octagonal and dodecagonal symmetry, the only other cases in two dimensions for which such analogues exist. The octagonal tiling is composed of two types of decorated tiles: a square and a 45° rhombus. The dodecagonal tiling is composed of three tile types: a regular hexagon, a square, and a 30° rhombus. Deflation procedures, matching rules, and Ammann-line decorations are explicitly displayed, secondary Ammann lines are defined and their significance with regard to the long-range order of the tilings is elucidated. The quasiperiodic sequences specifying the positions of the Ammann lines are derived and the appropriate projections from hypercubic lattices are described. Both the sufficiency of the matching rules and the equivalence of tilings produced by deflation and projection are demonstrated. The tilings are then used as a basis for a treatment of the elasticity of octagonal and dodecagonal quasicrystals. The irreducible phason strains are derived and the signatures of the different types of phason strain in real space and reciprocal space are determined. Standard analysis of a harmonic free energy reveals that there are three phason elastic constants for octagonal and dodecagonal quasicrystals (as opposed to two for decagonal ones) and there is no coupling of phason strain to conventional strain in the dodecagonal case. In each case, one linear combination of the phason elastic constants is irrelevant for phason fluctuations of wavelengths smaller than the sample size. Finally, some remarks are made concerning the applicability of standard elasticity theory to quasicrystals that are well described as simple decorations of tilings.

I. INTRODUCTION

The study of quasicrystal tilings with octagonal or dodecagonal orientational symmetry has become relevant for several reasons. The only noncrystallographic orientational symmetries observed to date in real materials are icosahedral, decagonal (or perhaps pentagonal), octagonal, and dodecagonal[1,2] and analysis of quasicrystal tilings of the plane indicates that these may be the only symmetries that support an ordered quasicrystalline phase.[3] In addition, studies of eightfold and twelvefold tilings may yield important information relating to gaps in our understanding of icosahedral and tenfold tilings. It is not known, for example, what determines the requisite complexity of matching rule decorations or what features of the tiling are necessary for the existence of a local growth algorithm. Comparison of the eightfold, tenfold, and twelvefold tilings is useful for determining whether relations that occur in the tenfold case are necessary or merely coincidental. The Penrose tilings[4] have played a special role in the study of decagonal quasicrystals because they display many remarkable properties in a particularly simple way. In this paper, octagonal and dodecagonal analogues of the Penrose tilings are presented and then used to illustrate certain features of the elasticity theory of octagonal and dodecagonal quasicrystals. It is shown that several techniques developed for the analysis of Penrose tilings can be carried over to these other symmetries.

It is possible to treat the cases of eightfold, tenfold, and twelvefold orientational symmetry together, since they share many essential properties. The most prominent feature that distinguishes these symmetries from all others in two dimensions is the appearance of quadratic irrationals in the ratios of incommensurate, collinear wave vectors in the diffraction pattern. [In two dimensions, $\cos(2\pi/Q)$ is a quadratic irrational only for $Q=5$, 8, 10, and 12.] As will become clear below, this allows similar constructions to be made in the different cases that greatly simplify the analysis. Each has a few unique features, so a complete analysis requires that they be treated separately at certain points, but the differences between the symmetries arise only in the detailed results; the same general concepts apply to all three cases.

The concepts of local isomorphism (LI) and orientational symmetry play an essential role in the analysis of quasicrystalline structure. In the literature, subtly different definitions of both terms have been used in order to emphasize different points, so it is necessary to give explicit definitions that will apply throughout this paper.

Local isomorphism. Two tilings are said to be *locally isomorphic* if and only if every finite region contained in either tiling can also be found (oriented the same way) in the other.[5] The set of all tilings locally isomorphic to a given tiling is the "LI class" of the tiling. All members of a given LI class have identical physical properties,[6] the distinct members being related by translations and phason shifts only.

Orientational symmetry. Let $\{g\}$ be the set of operations in the point group G. If for all g, operating with g on a tiling yields another tiling in the same LI class, and if G is the largest point group for which this is true, then G is the *orientational symmetry* of the tiling. In this paper, only tilings with symmorphic space groups are considered. For such tilings, an equivalent definition of orientational symmetry is as follows: A tiling is said to have a given point-group orientational symmetry if and only if there exists a member of its LI class whose diffraction pattern, *including phases,* is invariant under the symmetry operations of the point group. Note that under this definition, Penrose tilings (the original tilings introduced by Penrose[4,7]) have decagonal symmetry (even though they are often called "pentagonal quasicrystals"). Their point group is C_{10v} and they will be referred to as tenfold symmetric.

For any given orientational symmetry, it is possible to construct a multiply infinite number of quasicrystalline tilings, which can be grouped into LI classes.[6] For the case of tenfold symmetry, the original Penrose tilings form a single LI class (the "PLI class") that stands out as the most amenable to analysis. [Penrose tilings are infinite, space-fillng tilings of the plane with two types of oriented rhombus. An example is shown in Fig. 1(a)]. They possess the following four properties, which have been exploited in various ways to address issues in quasicrystal diffraction and elastic deformation,[1] facet formation,[8] growth,[9] and atomic structure.[1]

1. *Self-similarity.* There exists a "deflation" operation on any Penrose tiling that generates another Penrose tiling composed of smaller tiles, as well as an "inflation" operation that is the (unique) inverse of deflation.[4] Moreover, the deflation operation can be realized as a simple decoration of the original tiling, where "simple" means that every tile of a given shape is decorated the same way.

2. *Matching rules.* There exists a set of rules constraining the relative orientation of neighboring tiles in such a way that the only infinite space-filling tilings consistent with the rules are Penrose tilings.[4] These "matching rules" can be implemented via simple decoration of the tiles and a rule for how decorations on adjacent tiles must join.

3. *Ammann lines.* There exists a simple decoration of the tiles with line segments that join to form infinite straight lines in any Penrose tiling.[6] The infinite lines form five sets of parallel lines, each of which is called a "grid." The spacings between consecutive lines in each grid form a Fibonacci sequence of long and short intervals, so the equation of the Nth line in the nth grid can be written as

$$\mathbf{x}_{nN}\cdot\mathbf{e}_n = S\left[N+\alpha_n+\frac{1}{\tau}\left\lfloor\frac{N}{\tau}+\beta_n\right\rfloor\right], \tag{1}$$

where $\mathbf{e}_n \equiv (\cos(2\pi n/5),\ \sin(2\pi n/5))$, τ is the golden mean, $(1+\sqrt{5})/2$, α_n and β_n are constants, S is the length of the short interval, and the Iverson "floor function" $\lfloor x \rfloor$ denotes the greatest integer less than or equal to x. The requirement that the five grids taken together form a simple decoration of a Penrose tiling limits the number of degrees of freedom available in the choice of the α_n's and β_n's to four. (See Ref. 6.)

4. *Projection from a hypercubic lattice.* The vertices of a Penrose tiling can be obtained as the orthogonal projections of a subset of five-dimensional (5D) hypercubic lattice points onto a 2D plane.[10] The subset consists of all lattice points whose orthogonal projections onto the 3D complement of the tiling plane lie within the projection of a unit hypercube.

It should be emphasized that the special quality of the Penrose tilings is that properties 1–3 involve *simple* decorations. (See property 1 above.) This greatly simplifies the analysis of the tilings, but it does not distinguish them in any more fundamental sense. Other decagonal tilings do exhibit similar properties; it is just that analysis of them requires that distinctions be made between various tiles of the same shape, or, equivalently, that more than two types of tile be employed.

In this paper, PLI classes with eightfold and twelvefold symmetry (tilings having properties 1–4) are presented. The intent is to provide enough information so that the reader can exploit the properties of these tilings in investigating the physics of octagonal and dodecagonal quasicrystals. While other authors have considered tilings with these symmetries,[11–16] this is the first analysis that properly addresses the issues of matching rules and Ammann lines, as well as deflation and projection procedures. In addition, it is demonstrated here that certain general results of elasticity theory are reflected in these tilings in a natural way, the different irreducible phason strains having distinctive effects both in real space and reciprocal space. The nature of the defects associated with phason strain in the tilings raises questions about the relevance of standard treatments of their energetics.

We begin, in Sec. II, with a description of the Penrose tilings and their eightfold and twelvefold analogues. The section includes the information required for the reader to reproduce them and a discussion of some differences among the three symmetries. In Sec. III proofs of the assertions of Sec. II (proofs of properties 1–4 for the tilings) are provided, with some details relegated to appendixes. In Sec. IV, the subject of phason strains is treated, with an emphasis on the characterization of the different types of irreducible strains. In Sec. V the free energy associated with phason strains is discussed. Finally, in Sec.

VI, some implications of this work are suggested.

Throughout the paper, emphasis is placed on new results for the octagonal and dodecagonal tilings. The decagonal case has been treated extensively in the literature. It is assumed here that the reader is familiar with the basic properties of the Penrose tilings, including their construction via the generalized dual method (GDM) applied to periodic pentagrids[10] or Ammann quasilattices[5] and the strip projection method,[10,17] the effect of phason strain upon them,[18] and the structure of their diffraction patterns.[19,20] Results for the decagonal tilings are simply quoted here, when appropriate, for the purpose of comparison.

Two topics relevant to the octagonal and dodecagonal tilings that are *not* addressed here are the diffraction pattern and the nature of dislocations. General analyses of quasicrystal diffraction have appeared in the literature[1] and application of them to these two symmetries is straightforward. The analysis of the Burgers vector lattice that characterizes dislocations is so similar in all its details to the analysis of dislocations in Penrose tilings[18,21] that it is unnecessary to repeat it here.

II. DESCRIPTION OF THE PLI CLASS TILINGS

This section contains descriptions of the PLI class tilings, unencumbered by derivations of the properties they are claimed to have. Further discussion, including proofs

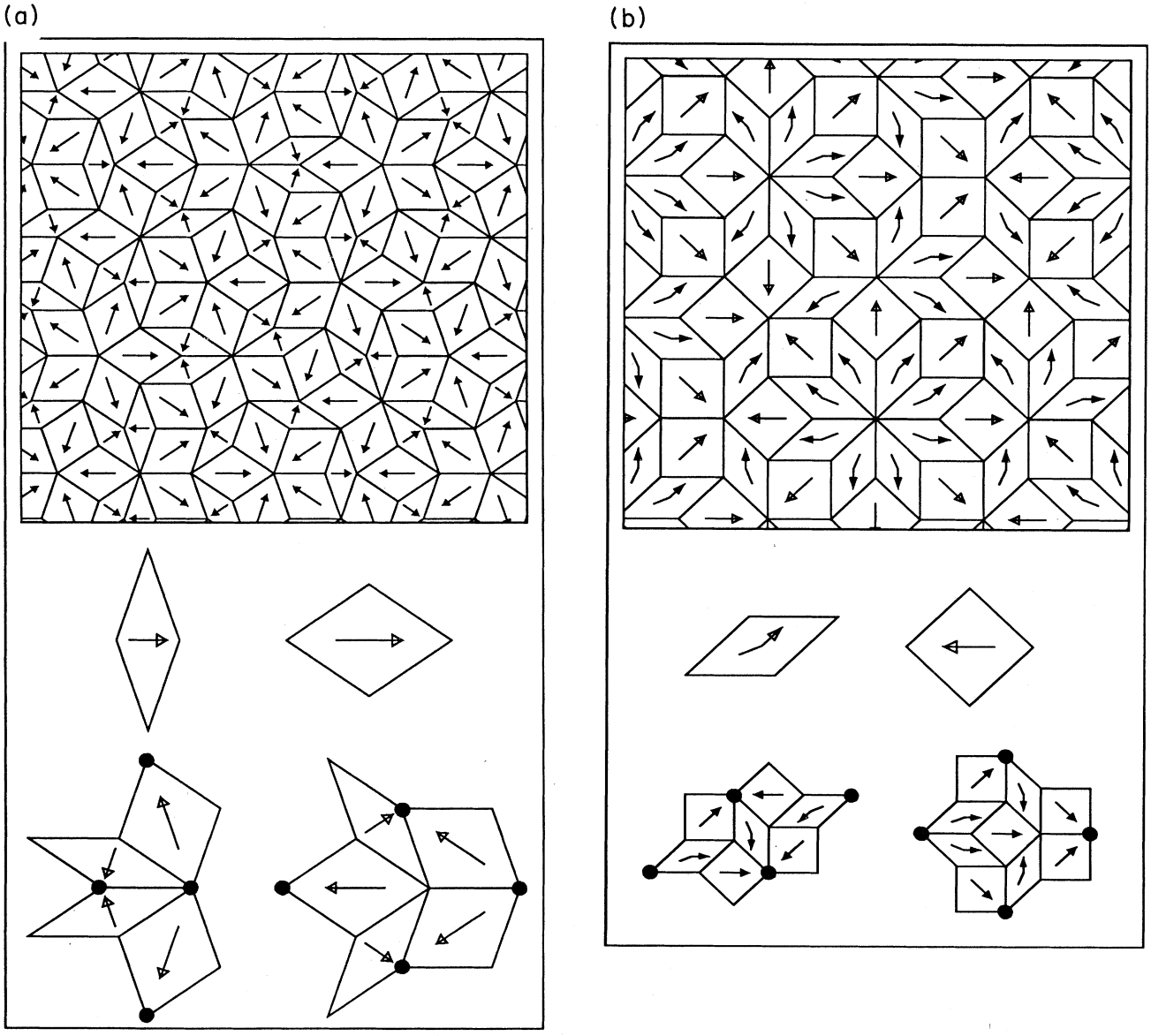

FIG. 1. The Penrose local-isomorphism (PLI) class tilings. The arrows on the tiles contain essential information about their orientations (see text). Below each tiling, a single tile of each type is displayed. Below them the result of the deflation procedure applied to single tiles with vertices at the solid dots is shown. The orientation of the deflations corresponds to the orientation of the arrows in the displayed single tiles. (a) Decagonal symmetry (the original Penrose tiling). (b) Octagonal symmetry (first discovered by Ammann). (c) Dodecagonal symmetry.

of the significant claims, can be found in Sec. III. Throughout the current section, references to the relevant subsections of Sec. III are given at the end of each paragraph. The absence of a reference indicates that the results discussed in that paragraph are straightforward (though perhaps tedious) to derive and are not discussed further.

A. Deflation rules

PLI class tilings with tenfold, eightfold, and twelvefold symmetry are shown in Fig. 1, along with the deflation rules that generate them. The arrows in the figure remove all ambiguities in the deflation prescription. If the arrows are ignored, there are certain tiles for which the deflation breaks the symmetry of the tile shape (tenfold tiles, the eightfold square, and the twelvefold hexagon). In order to deflate one of these tiles, one must know how the deflated configuration is to be oriented within the tile shape. The tiles have therefore been marked with arrows that indicate the orientation of the deflation decoration. Given the arrows on the hexagons, it is now found that the symmetry of the twelvefold square is broken, although it retains its mirror plane along one of its diagonals. The breaking of the diagonal symmetry of the twelvefold square and of both mirror symmetries in the eightfold and twelvefold rhombi is included in anticipation of the matching rule decorations, which require these distinctions.

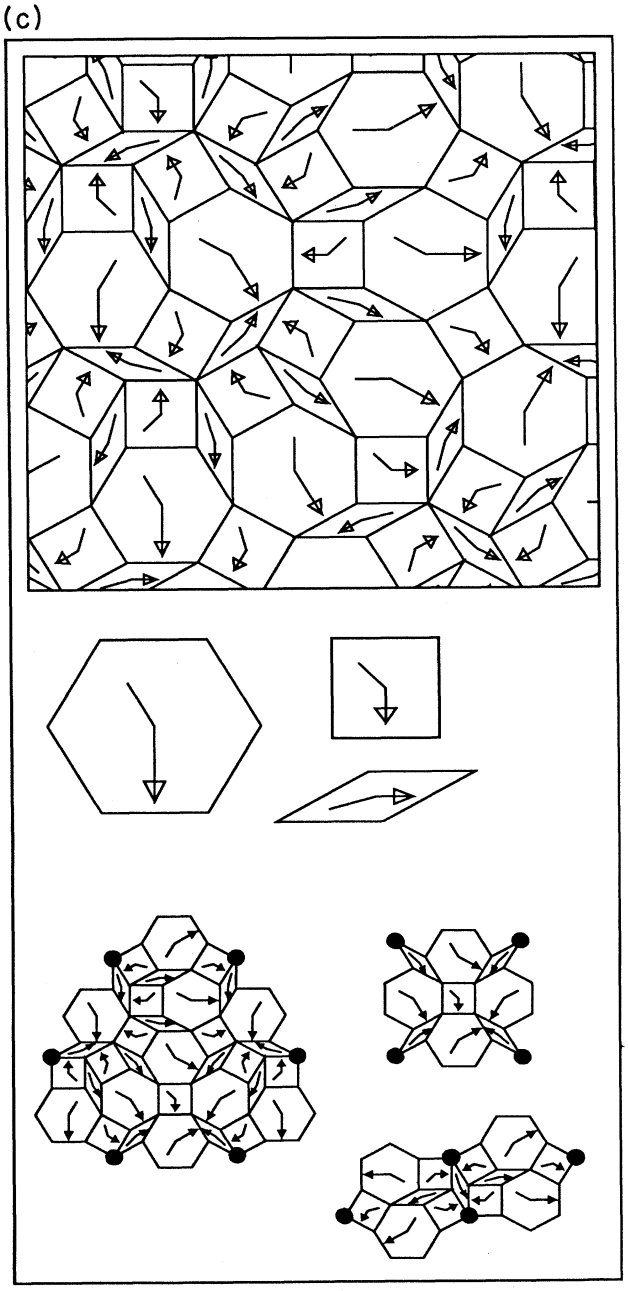

FIG. 1. (*Continued*).

It is the marked tiles that will be considered as the fundamental units of the tiling. To fully define the orientation of a tile, one must specify the orientation of the arrow as well as the orientation of the tile shape. The specification of the orientations of the deflated tiles is an essential element in the definition of the deflation procedure. A scheme must be found that is consistent with repeated deflation, and Fig. 1 shows the only such scheme, up to equivalent redefinitions of the arrow directions.

The orientational symmetry of the tiling requires that all tiles obtained from a given tile by a point-group operation must appear (with equal frequency) in the tiling. Since all the point groups under consideration contain mirror planes, any marked tile that does not have mirror symmetry must come in two versions, a "right-handed" and a "left-handed" version related by reflection. These two versions will generally be referred to as the same type of tile, although there is no rigid transformation that takes one into the other (in the 2D space of the tiling). The eightfold rhombus and all of the twelvefold tiles shown in Fig. 1 all have mirror image partners whose deflations are also mirror images of the ones depicted.

The ratio of the edge length of the original tiles, l, to the edge length of the deflated tiles, l^*, is

$$\frac{l}{l^*}=\begin{cases}\tau\equiv(1+\sqrt{5})/2 \text{ for the tenfold} & \text{(2a)}\\ \omega\equiv 1+\sqrt{2} \text{ for the eightfold} & \text{(2b)}\\ \xi\equiv 2+\sqrt{3} \text{ for the twelvefold .} & \text{(2c)}\end{cases}$$

The ratios of the frequencies of occurrence of the various tile types is easily determined from the deflation rules to be

$$\begin{aligned} &R_f{:}R_s=\tau{:}1, \quad S_8{:}R_8=1{:}\sqrt{2}\ ,\\ &H_{12}{:}S_{12}{:}R_{12}=1{:}\sqrt{3}{:}\sqrt{3}\ , \end{aligned} \tag{3}$$

Where R_f and R_s are the densities of fat and skinny rhombi in the tenfold tiling, S_8 and R_8 are the densities of the squares and 45° rhombi in the eightfold, and H_{12}, S_{12}, and R_{12} are the densities of the hexagons, squares, and 30° rhombi in the twelvefold. In every case, the frequencies of mirror-image partners are the same (Sec. III B 7).

B. Ammann quasilattices

The decoration of the PLI class tilings with Ammann lines is shown in Fig. 2. For the case of Q-fold symmetry, the Ammann lines form $Q/2$ grids (sets of parallel lines). In each grid, the sequence of spacings between successive lines is a quasiperiodic sequence of two lengths, T_Q and S_Q. The equations of the Ammann lines can be written as follows: Let $\mathbf{e}_n$ and $\bar{\mathbf{e}}_n$ be defined as shown in Fig. 3 and let $\mathbf{x}_{nN}$ be a point on the Nth line in the grid with lines perpendicular to $\mathbf{e}_n$. Then

$$\mathbf{x}_{nN}\cdot\mathbf{e}_n=\begin{cases} S_{10}\left[N+\alpha_n+\dfrac{1}{\tau}\left\lfloor\dfrac{N}{\tau}+\beta_n\right\rfloor\right], & n=0,1,2,3,4 \text{ (tenfold)}, \quad (4a)\\ S_8\left[N+\alpha_n+\dfrac{1}{\omega}\left\lfloor\dfrac{N}{\omega}+\beta_n\right\rfloor\right], & n=0,1,2,3 \text{ (eightfold)}, \quad (4b)\\ S_{12}\left[N+\alpha_n-\dfrac{1}{\xi}\left\lfloor\dfrac{N}{\xi}+\beta_n\right\rfloor\right], & n=0,1,2,3,4,5 \text{ (twelvefold)}, \quad (4c)\end{cases}$$

with

$$\alpha_n=\begin{cases} \dfrac{1}{2\tau}+\mathbf{u}+\mathbf{e}_n+p_n+q_n/\tau \text{ (tenfold)}, & (5a)\\ \dfrac{1}{2\omega}+\mathbf{u}\cdot\mathbf{e}_n+p_n+q_n/\omega \text{ (eightfold)}, & (5b)\\ \dfrac{-1}{2\xi}+\mathbf{u}\cdot\mathbf{e}_n+p_n-q_n/\xi \text{ (twelvefold)}, & (5c)\end{cases}$$

$$\beta_n=\begin{cases} \mathbf{w}\cdot\bar{\mathbf{e}}_n-q_n+p_n/\tau \text{ (tenfold)} & (5a')\\ \mathbf{w}\cdot\bar{\mathbf{e}}_n-q_n+p_n/\omega \text{ (eightfold)} & (5b')\\ \mathbf{w}\cdot\bar{\mathbf{e}}_n-q_n+p_n/\xi \text{ (twelvefold)}, & (5c')\end{cases}$$

where $\mathbf{u}$ and $\mathbf{w}$ are arbitrary vectors and p_n and q_n are arbitrary integers. Note that the expressions for α_n and β_n contain the same p_n and q_n. (Section III B 2).

The union of the $Q/2$ Ammann line grids will be called

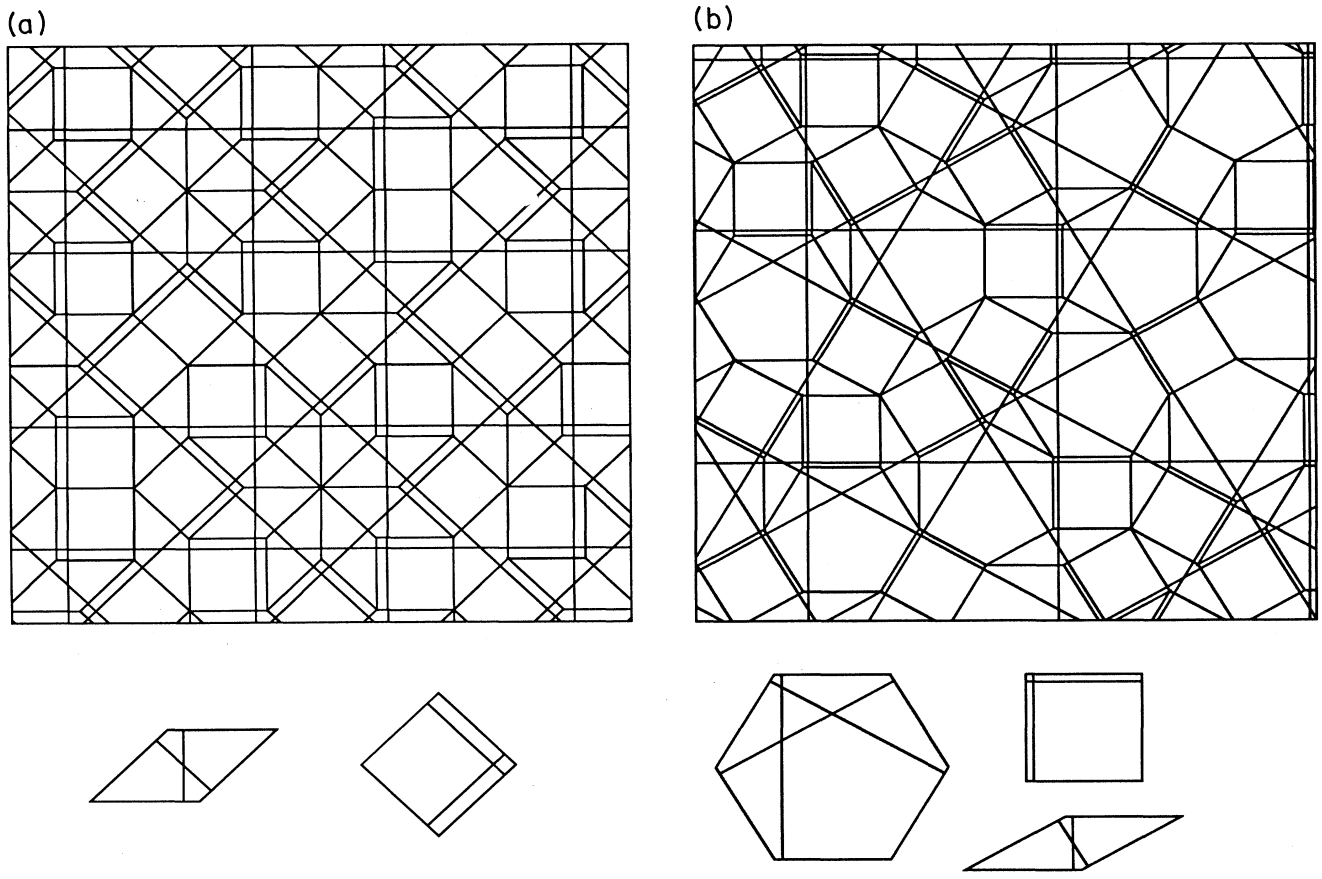

FIG. 2. Primary Ammann-line decorations. The orientations of the displayed single tiles are identical to those in Fig. 1.

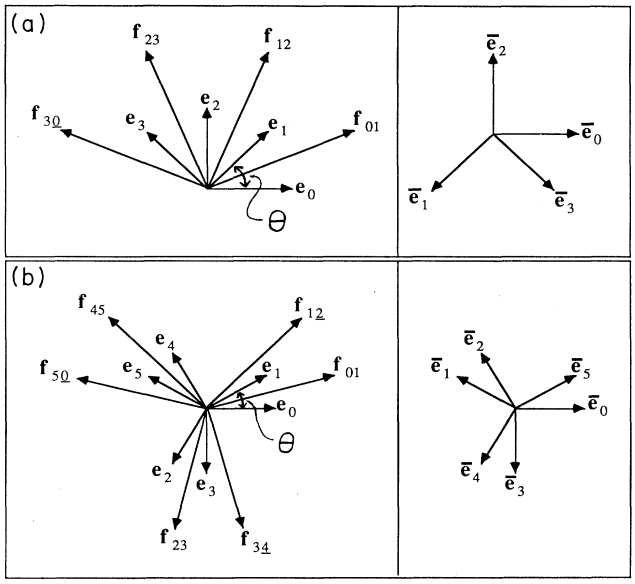

FIG. 3. Definitions of vectors $\mathbf{e}_n$, $\bar{\mathbf{e}}_n$, and $\mathbf{f}_{nm}$. (a) Octagonal symmetry: $\theta=\pi/4$; $\mathbf{e}_n=(\cos(n\theta),\sin(n\theta))$; $\bar{\mathbf{e}}_n=\mathbf{e}_{5n\,(\mathrm{mod}\,8)}$. (b) Dodecagonal symmetry: $\theta=\pi/6$; $\mathbf{e}_n=(\cos(n\theta),\sin(n\theta))$ for $n=0,1,4,5$; $\mathbf{e}_n=-(\cos(n\theta),\sin(n\theta))$ for $n=2,3$; $\bar{\mathbf{e}}_n=\mathbf{e}_{5n\,(\mathrm{mod}\,12)}$. [See text (Sec. III B) for definition of $\mathbf{f}_{nm}$.]

the *Ammann quasilattice*. Different values of $\mathbf{u}$ in Eq. (5) simply produce Ammann quasilattices related by an overall translation. Different values of $\mathbf{w}$ produce different Ammann quasilattices belonging to tilings in the same LI class; i.e., tilings related by a *uniform phason shift*. The values of S_Q are

$$S_{10}=\frac{\sqrt{5}}{2},\quad S_8=1+\frac{\sqrt{2}}{2},\quad S_{12}=\tfrac{3}{2}+\sqrt{3}\ , \tag{6}$$

where the length of a tile edge is taken to be unity.

Note that Eqs. (4) and (5) are all of the form

$$\begin{aligned}
&\mathbf{x}_{nN}\cdot\mathbf{e}_n=S_Q\left[N+\alpha_n+\frac{1}{\sigma'}\left\lfloor\frac{N}{\sigma}+\beta_n\right\rfloor\right],\\
&\alpha_n=\frac{1}{2\sigma'}+\mathbf{u}\cdot\mathbf{e}_n+p_n+q_n/\sigma'\ ,\\
&\beta_n=\mathbf{w}\cdot\bar{\mathbf{e}}_n-q_n+p_n/\sigma\ ,
\end{aligned} \tag{7}$$

where $\sigma=\tau$, ω, or ξ and $\sigma'=\tau$, ω, or $-\xi$ for the cases of tenfold, eightfold, and twelvefold symmetry, respectively. For the remainder of this paper, whenever a formula can be written so as to apply to all three cases simultaneously, we will use σ and σ' rather than writing out each of the cases. For example, we can write the ratio of the two different intervals between Ammann lines as $T_Q/S_Q=1+1/\sigma$.

A property of the Ammann quasilattice that has proven useful for a variety of purposes is that its "dual" tiling, defined according to the generalized dual method,[22] is very simply related to the tiling that is decorated to form the Ammann quasilattice. In the tenfold case, the dual of the Ammann quasilattice is the deflation of the original tiling.[5] In both the eightfold and twelvefold cases, the dual of the Ammann quasilattice is precisely the original tiling. In the eightfold case, this is obvious from the Ammann-line decoration (Fig. 2). There is a one-to-one correspondence between the tiles and the Ammann-line intersections. Furthermore, for each tile, the orientation and shape of the tile correspond exactly to the dual of the Ammann-line intersection in its interior. In the twelvefold case, the correspondence between the squares and rhombi and their dual Ammann-line intersections is apparent. In the hexagon, there are three Ammann-line intersections whose duals, strictly speaking, are three 60° rhombi. Such rhombi always occur grouped together to form hexagons, and so it is simpler to view the hexagon as a single unit. (A good reason for doing so becomes apparent when the tiling is constructed as the dual to a periodic 6-grid, as discussed below.)

For reasons that will become apparent in the discussions of matching rules and phason strains, it is useful to define another decoration of the eightfold and twelvefold tilings. Decorations of the tilings with "secondary Ammann lines" are shown in Fig. 4. (Henceforth, the original Ammann quasilattice will be referred to as the "primary" Ammann quasilattice.) The fact that the secondary Ammann-line decoration of each tile extends beyond the tile boundary must be accepted if one insists upon a simple decoration. It should also be noted that when the decorated tiles are joined to form the PLI class tiling, the decoration line segments do not all join just at their endpoints; in some cases they overlap.

In order to obtain a compact form for the equations of the lines in the secondary Ammann quasilattice, the following definitions are made (see Fig. 3):

$$\begin{aligned}
&\beta_{\underline{n}}\equiv-\beta_n\ ;\\
&\alpha_{\underline{n}}\equiv-\alpha_n+\frac{1}{\sigma'}\\
&\mathbf{f}_{nm}\equiv\begin{cases}\mathbf{e}_n+\mathbf{e}_m,\quad \mathbf{e}_4\equiv-\mathbf{e}_0,\quad n=0,1,2,3\ \text{(eightfold)}\ ,\\ \mathbf{e}_n+(-1)^{m+1}\mathbf{e}_n,\quad \mathbf{e}_6\equiv\mathbf{e}_0, n=0,1,2,3,4,5\ \text{(twelvefold)}\ .\end{cases}
\end{aligned} \tag{8}$$

$\alpha_{\underline{n}}$ and $\beta_{\underline{n}}$ are defined such that the grid defined by $\mathbf{x}\cdot(-\mathbf{e}_n)=N+\alpha_{\underline{n}}+1/\sigma'\lfloor n/\sigma+\beta_{\underline{n}}\rfloor$ is identical to that defined by $\mathbf{x}\cdot\mathbf{e}_n=N+\alpha_n+1/\sigma'\lfloor N/\sigma+\beta_n\rfloor$.

The equations of the secondary Ammann lines for the tiling defined by Eqs. (4) and (5) are

$$\mathbf{x}\cdot\mathbf{f}_{nm} = = \begin{cases} S_8\left[N+\alpha_{nm}+\dfrac{1}{\omega}\left\lfloor\dfrac{N}{\omega}+\beta_{nm}\right\rfloor\right] & nm=01,12,23,3\underline{0}\ \text{(eightfold)}\ , \\ S_{12}\left[N+\alpha_{nm}-\dfrac{1}{\xi}\left\lfloor\dfrac{N}{\xi}+\beta_{nm}\right\rfloor\right] & nm=01,1\underline{2},23,3\underline{4},45,5\underline{0}\ \text{(twelvefold)}\ , \end{cases} \tag{9}$$

where

$$\beta_{nm}=\beta_n+\beta_m \quad \text{and} \quad \alpha_{nm}=\alpha_n+\alpha_m-\frac{1}{2\sigma'}\ . \tag{10}$$

The secondary Ammann quasilattice is locally isomorphic to the primary Ammann quasilattice rotated by π/Q and scaled down by a factor of $\|\mathbf{e}_0+\mathbf{e}_1\|$. (Secs. III B 3 and III B 4).

There is a simple interpretation of the primary and secondary Ammann lines as analogues of Bragg planes in periodic crystals. Peak positions in the Fourier transforms of decorations of the tenfold, eightfold, and twelvefold tilings lie at wavevectors $\mathbf{q}=\sum_n k_n\mathbf{e}_n$, sometimes denoted $(k_0k_1\ldots)$, where k_n is any integer. (Note that this labeling is redundant in the tenfold and twelvefold cases since $(11111)=0$ in the tenfold case and $(101010)=(010101)=0$ in the twelvefold case.) Diffraction from a single grid of primary Ammann lines, the lines perpendicular to $\mathbf{e}_0$ for example, would produce the familiar one-dimensional Fourier transform of the quasiperiodic sequence in the $(100\ldots)$ direction, just as diffraction from a single set of Bragg planes normal to the x axis produces peaks in the (100) direction. In the same sense, the secondary Ammann lines are associated with peaks in the $(1100\ldots)$ directions.

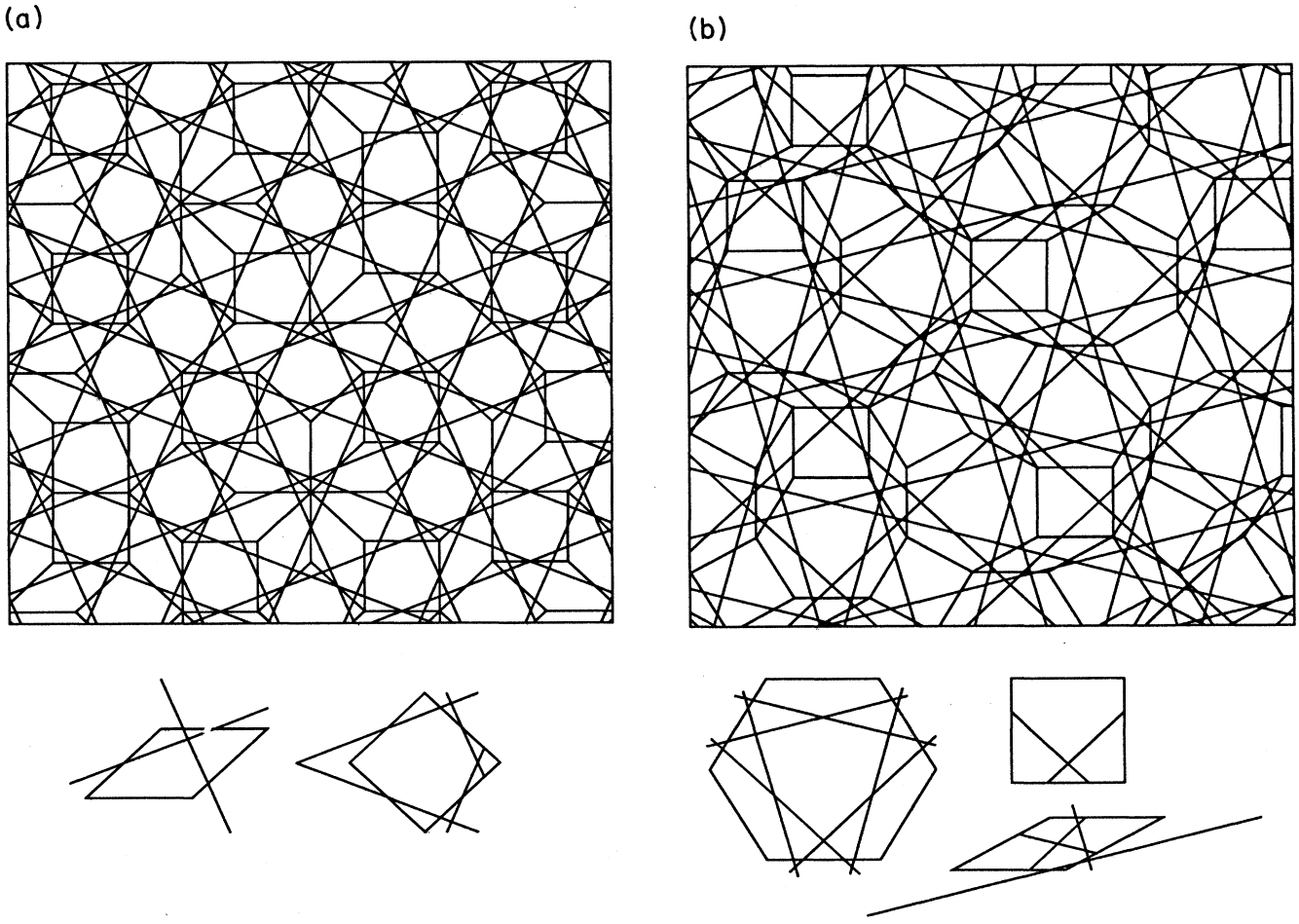

FIG. 4. Secondary Ammann line decorations. The orientations of the displayed single tiles are identical to those in Fig. 1. Note that decorations of individual tiles extend beyond the tile boundary.

C. Matching rules

Matching rules for the eightfold and twelvefold PLI class tilings are shown in Fig. 5. Both cases are similar to the tenfold case[5] in that the rule that a single triangle must be formed along each edge in the tiling is equivalent to the requirement that primary Ammann lines be continuous, infinite, and straight. In the tenfold case, forcing the primary Ammann lines to be continuous and straight is sufficient to force nonperiodicity, but in the eightfold and twelvefold cases an additional rule is needed. The black shape formed at each vertex must be identical (up to rotations) to the "key" shown in Fig. 5. Constraining these vertex keys to have the right shape ensures the continuity of the secondary Ammann lines and, together with the edge restrictions, guarantees that any infinite, space-filling tiling is in the PLI class (Sec. III B 5).

The use of a rule that constrains the orientations of tiles that share only a vertex in common is not absolutely necessary. Matching rules that apply only across tile edges can be derived from the secondary Ammann-line decoration; the catch is that many types of decorated

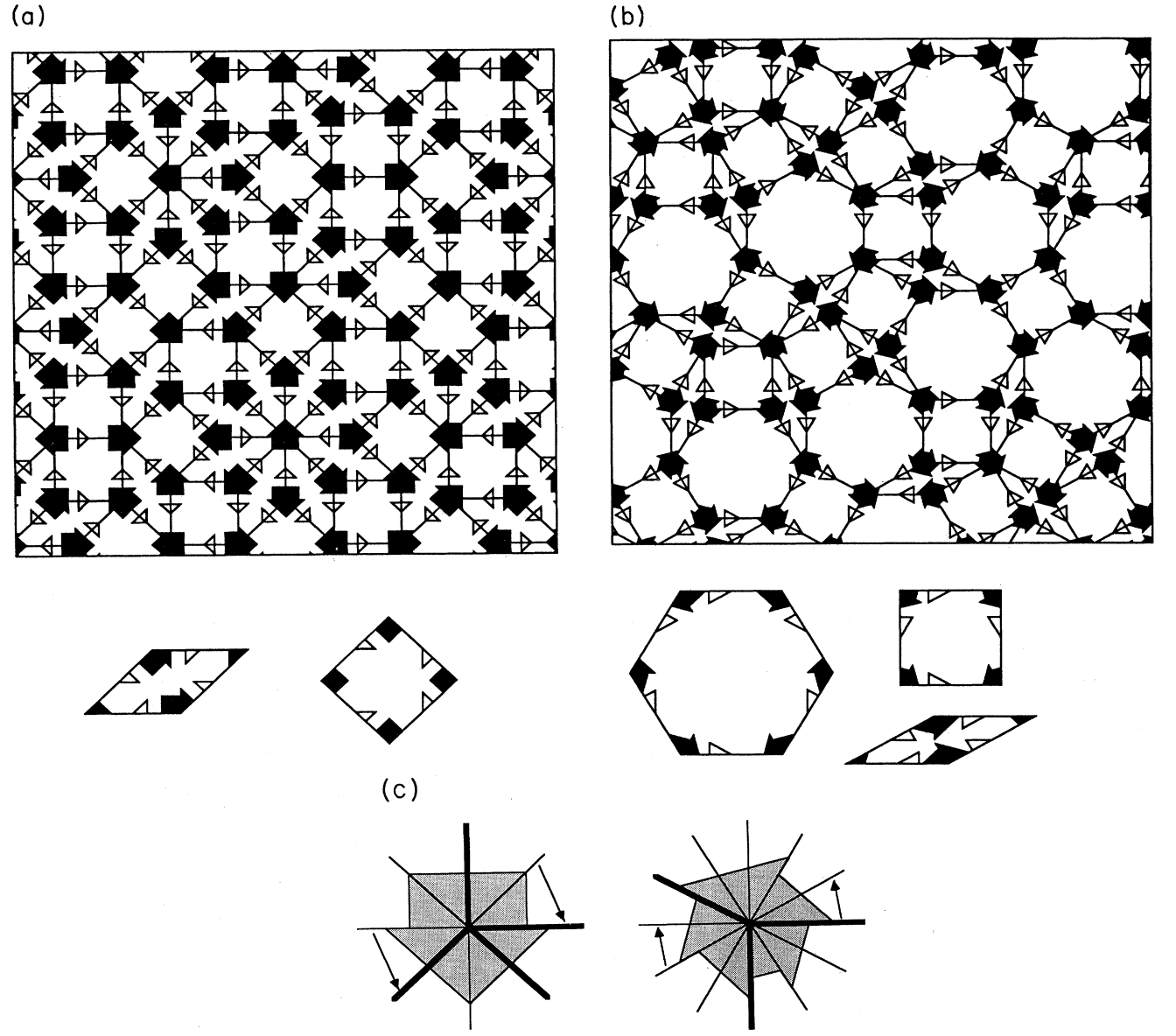

FIG. 5. Matching rule decorations. The orientations of the displayed single tiles are identical to those in Fig. 1. The shape of the key that must be formed at every vertex is shown in black. (a) Octagonal symmetry. (Rules first discovered by R. Ammann.) (b) Dodecagonal symmetry. (c) The vertex keys of the eightfold and twelvefold matching rules. The thick lines are tile edges at a typical vertex. The other radial lines are included to elucidate the structure of the key. Note that in both cases, the segments of the key that lie opposite each other (the ones marked with arrows, for example) are related by a single reflection, never by a full inversion (i.e., the arrows point in the same direction).

squares, rhombi, and hexagons must be defined; i.e., the decoration is no longer simple. This decoration can be constructed by inspection of a tiling decorated with both primary and secondary Ammann lines. Since parts of the secondary Ammann-line decoration of Fig. 5 extend beyond the tile borders, tiles of the same type appear to have different decorations, depending on their local environments. If the figure is now viewed as being composed of tiles with decorations that do not extend beyond their borders, many types of tiles can be identified. For the eightfold case, there are nine types—four 45° rhombi (and their mirror) images plus five squares (three of which have distinct mirror images). For the twelvefold case, there are thirteen types—three rhombi, five squares, and five hexagons (all of which have distinct mirror images).

D. Projection from a hypercubic lattice

It is well known that the vertices of the Penrose tilings can be generated by orthogonal projection of a 5D hypercubic lattice onto a properly oriented 2D plane[10] and it is assumed here that the reader is familiar with this construction. As one might expect, the eightfold PLI class can be obtained as the projection of a 4D hypercubic lattice and the twelvefold from a 6D hypercubic lattice. The following notation will be used in discussing the projections for the case of Q-fold symmetry ($Q=8,10,12$).

E: The $(Q/2)$-dimensional space of the hypercubic lattice.

$\mathbf{R}$: A generic point in the hypercubic lattice.

$\mathbf{b}_n$ ($n=0,1,\ldots Q/2-1$): The basis vectors of the hypercubic lattice: $\mathbf{b}_0=(100\cdots)$, $\mathbf{b}_1=(010\cdots)$, etc.

$E^{\parallel}$: A 2D subspace of E, chosen such that the orthogonal projection of $\mathbf{b}_n$ onto $E^{\parallel}$ is $\mathbf{e}_n$ (defined in Fig. 3). $E^{\parallel}$ is the "physical space" of the tiling.

$E^{\perp}$: The orthogonal complement of $E^{\parallel}$ in E (sometimes referred to as "perp-space").

$\bar{E}$: A 2D subspace of $E^{\perp}$, chosen such that the orthogonal projection of $\mathbf{b}_n$ onto $\bar{E}$ is $\bar{\mathbf{e}}_n$ (defined in Fig. 3).

$E^{(\mathrm{LI})}$: The orthogonal complement of $\bar{E}$ in $E^{\perp}$. (For the eightfold case $E^{(\mathrm{LI})}$ is null.)

$P^{\parallel},P^{\perp},\bar{P},P^{(\mathrm{LI})}$: Matrices that project onto $E^{\parallel},E^{\perp},\bar{E}$, and $E^{(\mathrm{LI})}$, respectively:

$$P^{\parallel}_{ij}=\sqrt{2/Q}\,\mathbf{e}_i\cdot\mathbf{e}_j,\quad \bar{P}_{ij}=\sqrt{2/Q}\,\bar{\mathbf{e}}_i\cdot\bar{\mathbf{e}}_j\ ,$$

$$P^{\perp}=I-P^{\parallel},\quad P^{(LI)}=P^{\perp}-\bar{P}\ .$$

$\mathbf{z},\mathbf{z}^{\parallel},\mathbf{z}^{\perp},\bar{\mathbf{z}},\mathbf{z}^{(\mathrm{LI})}$: An arbitrary point in E and its projections onto the various subspaces. $\mathbf{z}^{\parallel}=P^{\parallel}\mathbf{z}$, etc.

$C^{\perp}$: The image of the unit hypercube in $E^{\perp}$. $C^{\perp}$ is the set of $\mathbf{z}^{\perp}$ obtained from all $\mathbf{z}$ satisfying $0\le\mathbf{z}\cdot\mathbf{b}_n<1,\forall n$.

The vertices of the tiles in $E^{\parallel}$ are the points $P^{\parallel}(\mathbf{R}+\mathbf{g})$, where $\mathbf{g}$ is an arbitrary vector and $P^{\perp}(\mathbf{R}+\mathbf{g})\in C^{\perp}$. The choice of $\mathbf{g}$ fully specifies the tile positions. The different terms in the decomposition $\mathbf{g}=\mathbf{g}^{\parallel}+\bar{\mathbf{g}}+\mathbf{g}^{(\mathrm{LI})}$ have distinct meanings. Uniform shifts in $\mathbf{g}^{\parallel}$ correspond to overall translations of the tiling in $E^{\parallel}$; uniform shifts in $\bar{\mathbf{g}}$ to shifts between different members of the same LI class (phason shifts); and uniform shifts in $\mathbf{g}^{(\mathrm{LI})}$ to shifts between LI classes. For particular choices of $\mathbf{g}^{(\mathrm{LI})}$, the tilings produced by projection are identical to those produced by deflation or by taking the dual of an Ammann quasilattice (Sec. III B 6).

The different symmetries must now be treated separately.

Tenfold: The Penrose case has been treated in detail in the literature.[10] $E^{(\mathrm{LI})}$ is the 1D space spanned by the vector (11111). Let Γ be the sum of the components of $\mathbf{g}^{(\mathrm{LI})}$. There are two values of $\mathrm{mod}_1\Gamma$, namely 0 and $\frac{1}{2}$, that give tilings with tenfold symmetry; all others give tilings with only fivefold symmetry. The value corresponding to the Penrose tilings are $\mathrm{mod}_1\Gamma=0$. Note that, although $C^{\perp}$ is three dimensional, the projected lattice points $P^{\perp}\mathbf{R}$ lie in 2D planes that are filled densely and uniformly.[10,17] In general, five of these planes intersect $C^{\perp}$ in more than a single point. In the case of a Penrose tiling, however, only four of them do.

Eightfold: In this case, $E^{\parallel}$ and $\bar{E}$ exhaust E, so there is no $E^{(\mathrm{LI})}$. $C^{\perp}$ is an octagon lying in $\bar{E}$, filled densely and uniformly by $\bar{P}(\mathbf{R}+\mathbf{g})$. Points in different regions of $C^{\perp}$ correspond to different types of vertices in the tiling, as shown in Fig. 6. The type of vertex is determined as follows. If, for a given point $z^{\perp}\in C^{\perp}$, the point $\mathbf{z}^{\perp}\pm\bar{\mathbf{e}}_n$ is also in $C^{\perp}$, then there is an edge in the $\pm\mathbf{e}_n$ direction emanating from the vertex at $\mathbf{z}^{\parallel}$.

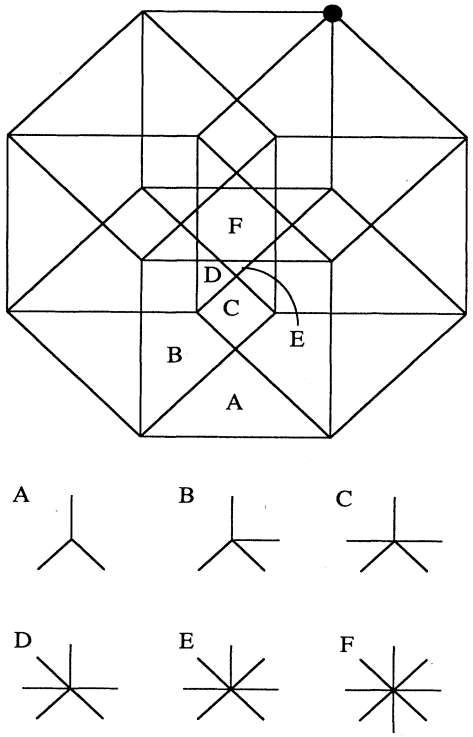

FIG. 6. Perp-space structure of octagonal PLI class tiling. Above: The projection of the 4D unit hypercube onto the 2D perp-space. Letting $(k_0k_1k_2k_3)$ represent $\sum_r k_n\mathbf{e}_n^{\perp}$, the vertices of the large octagon, beginning with the solid dot and moving clockwise, are (1010), (1011), (1001), (1101), (0101), (0100), (0110), and (0010). Below: The configuration of edges around vertices in the tiling corresponding to points in each of the labeled regions.

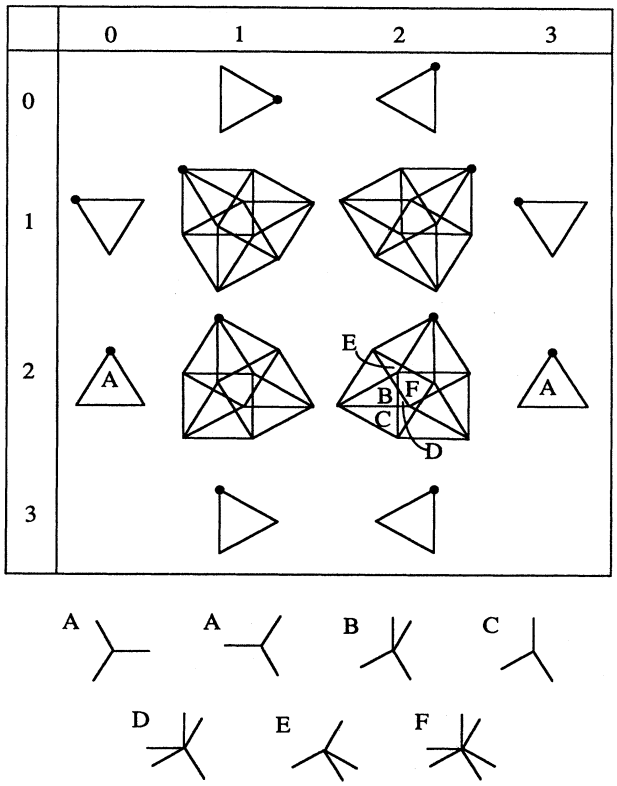

FIG. 7. Perp-space structure of dodecagonal PLI class tiling. Above: The projection of the 6D unit hypercube onto the 4D perp-space. Only the intersection of the projection with planes defined by $\sum_{n=1,3,5}\mathbf{x}^{\perp}\cdot\mathbf{e}_n^{\perp}=i$ and $\sum_{n=0,2,4}\mathbf{x}^{\perp}\cdot\mathbf{e}_n^{\perp}=j$, where i and j are integers. Each row in the table corresponds to the indicated value of i, each column to the indicated j. Letting $(k_0k_1k_2k_3k_4k_5)$ represent $\sum_r k_n\mathbf{e}_n^{\perp}$, the vertices on the perimeters of each entry in the table, beginning with the solid dot and moving clockwise, are

$(ij)=(01)$: (100000),(000010),(001000) .
$(ij)=(02)$: (101000),(100010),(001010) .
$(ij)=(10)$: (010000),(000001),(000100) .
$(ij)=(20)$: (010001),(000101),(010100) .
$(ij)=(13)$: (111010),(101011),(101110) .
$(ij)=(23)$: (111011),(101111),(111110) .
$(ij)=(31)$: (011101),(110101),(010111) .
$(ij)=(32)$: (111101),(110111),(011111) .
$(ij)=(11)$: (011000),(001001),(100001) ,
(100100),(000110),(010010) .
$(ij)=(12)$: (101001),(100011);(100110) ,
(001110),(011010),(111000) .
$(ij)=(21)$: (011001),(110001),(100101) ,
(0001111),(010110),(011100) .
$(ij)=(22)$: (111001),(101101),(100111) ,
(110110),(011110),(011011) .

Below: The configuration of edges around vertices in the tiling corresponding to points in each of the labeled regions.

Twelvefold: Here $E^{(\mathrm{LI})}$ is two dimensional and is panned by $\mathbf{e}_1^{(\mathrm{LI})}\equiv(010101)$ and $\mathbf{e}_2^{(\mathrm{LI})}\equiv(101010)$. Let (a,b) denote the pair $[\mathrm{mod}_1(\mathbf{g}^{(\mathrm{LI})}\cdot\mathbf{e}_1^{(\mathrm{LI})}),\ \mathrm{mod}_1(\mathbf{g}^{(\mathrm{LI})}\cdot\mathbf{e}_2^{(\mathrm{LI})})]$. The tilings corresponding to (0,0) and $(\frac{1}{2},\frac{1}{2})$ have twelvefold symmetry, those corresponding to $(0,\frac{1}{2})$ and $(\frac{1}{2},0)$ have sixfold symmetry, and the rest have only threefold symmetry. The PLI class tilings are produced by (0,0). The projected lattice points fill 2D planes that intersect $C^{\perp}$ to form twelve polygons in the PLI case, as shown in Fig. 7. The triangular regions residing in the (0,1), (0,2), (1,0), (2,0), (3,1), (3,2), (1,3), and (2,3) planes represent vertices shared by three 60° rhombi that can always be grouped to form a hexagon. Eliminating these pieces of $C^{\perp}$ produces the PLI class tiling with hexagons, squares, and rhombi.

The derivations of the "perp-space" structure of the projected eightfold and twelvefold tilings are straightforward, and similar enough to well-known analysis of the tenfold case that they need not be detailed in this paper.

The projection construction is completely equivalent to the application of the GDM to periodic N-grids.[23] (A periodic N-grid is defined by $\mathbf{x}_{nM}\cdot\mathbf{e}_n=M+\gamma_n$, $n=0,1,\ldots,N-1$.) The PLI class tilings can all be produced by the GDM applied to periodic $(Q/2)$-grids. The above results for projections can be translated directly into their GDM counterparts: the nth component, γ_n, of $\mathbf{g}$ is the distance to the origin of one of the lines in the periodic grid with normal $\mathbf{e}_n$. The tenfold Penrose tilings correspond to $\sum_n\gamma_n=0$ (mod 1). In the eightfold case there is no restriction on γ_n. In the twelvefold case, the PLI class is given by $\gamma_0+\gamma_2+\gamma_4=\gamma_1+\gamma_3+\gamma_5=0$ (mod 1). The periodic 6-grid in this case is singular at every intersection of grids 0, 2, and 4, or grids 1, 3, and 5, each of these triplets of grids forming a triangular lattice. The duals of the singular intersections are the hexagons in the tiling. The method of taking the dual of two overlapping triangular lattices was the technique used by Ammann, who first produced the twelvefold PLI class tiling,[12] and it provides the aforementioned reason for considering the hexagon as a single unit.

III. PROOFS OF THE PLI CLASS PROPERTIES

A. Definitions and outline of reasoning

This section contains derivations of the results presented in Sec. II. We begin by determining the values of α_n and β_n that define the Ammann quasilattice. We then show that the dual to the Ammann quasilattice has the deflation, matching rule, and projection properties that characterize the PLI class. The following definitions and notation are employed.

(i) For the purposes of this paper, a *quasiperiodic grid* is a set of parallel lines with the points $\mathbf{x}_N$ on the line with (integer) index N defined by

$$\mathbf{x}_N\cdot\mathbf{e}=S\left[N+\alpha+\frac{1}{\sigma'}\left\lfloor\frac{N}{\sigma}+\beta\right\rfloor\right], \tag{11}$$

where σ and σ' are the values appropriate to either the eightfold, tenfold or twelvefold Ammann quasilattices and $\mathbf{e}$ is a fixed vector called a *star vector*. ($\sigma=\sigma'=\tau$, $\sigma=\sigma'=\omega$, or $\sigma=-\sigma'=\xi$.) This is not the most general form for quasiperiodic grids, but it covers the cases of interest here. The spacing between consecutive lines in the grid is either S or $T\equiv S(1+1/\sigma')$. (α,β) denotes a quasiperiodic grid with specified values of the parameters α and β.

(ii) A *quasiperiodic M-grid* is the union of M quasiperiodic grids with M different star vectors. Each grid is determined by its star vector, $\mathbf{e}_n$, the parameters α_n and β_n, and the values of σ and σ'. We will be concerned only with 4-grids and 6-grids with $\mathbf{e}_n$'s defined by Fig. 3. (5-grids are treated in Ref. 5.) $\{\alpha_n,\beta_n\}$ denotes a specific quasiperiodic M-grid.

(iii) In keeping with the convention of Ref. 5, two M-grids are called locally isomorphic if the tilings dual to them are locally isomorphic. If the M-grids themselves satisfy the conditions of local isomorphism, they are called *locally congruent.*

(iv) An *Ammann quasilattice* is a quasiperiodic M-grid with α_n and β_n chosen such that its dual tiling is in the PLI class.

(v) The *unscaled deflation* of a tiling is the result of dividing the tiles into smaller ones according to a deflation operation. The *rescaled deflation* is the result of rescaling the lengths in the unscaled deflation so that the tiles have the same size as those in the original tiling. Quasiperiodic grids can also be deflated, and (α^*,β^*) specifies the *rescaled* deflation of (α,β).

(vi) A *periodic M-grid* is composed of periodic grids defined by $\mathbf{x}_{Nn}\cdot\mathbf{e}_n=N+\gamma_n$ (where $n=1,2,\ldots,M$) and is denoted by $\{\gamma_n\}$.

Imagine now that we do not know what the eightfold or twelvefold PLI class tilings look like (or whether they even exist) and we wish to derive them. The method Penrose used in discovering the tenfold PLI class, construction of a deflation operation by trial and error, requires inspired guesswork. Two other approaches seem more promising. The first is to construct the tilings corresponding to the simplest choice of parameters in the projection method or the GDM. Deflation transformations can then be derived by inspection or by investigation of a certain class of operations on the acceptance volume, $C^{\perp}$, and Ammann lines could be constructed by inspection and trial and error. The second approach would be to construct the Ammann quasilattice directly, using the constraints imposed by the PLI class properties to determine the values of $\{\alpha_n,\beta_n\}$, and then take the dual of the Ammann quasilattice to form the tiling. It could then be determined whether or not the tiling corresponded to the projection of a hypercubic lattice. The latter approach will be used here because it provides the most direct insight into the nature of the matching rules and the phason strains discussed in Sec. IV, but neither approach can be claimed to have logical priority.

The line of reasoning used in establishing the PLI class properties is as follows.

(i) Define the deflation of a single quasiperiodic grid by analogy with the Penrose case. The form of the deflation operation will determine the values of σ and σ' in Eq. (11).

(ii) Derive the relation between the parameters of locally congruent quasiperiodic N-grids.

(iii) Derive the values of α_n and β_n for which the rescaled deflation of the individual grids produces a quasiperiodic N-grid that is locally congruent to the original. As is shown for the case of tenfold symmetry in Ref. 5, this criterion selects the Ammann quasilattices from among all possible quasiperiodic N-grids.

(iv) Determine the deflation rule induced on the tilings dual to the Ammann quasilattices. The direct deflation of the Ammann quasilattice will induce the deflation operations depicted in Fig. 1 (although the orientations of the marked tiles will not be specified).

(v) Demonstrate that the secondary Ammann quasilattice decoration is consistent with all tilings produced by the deflation operation.

(vi) Derive the values of α_{nm} and β_{nm} for the secondary Ammann quasilattice in terms of α_n and β_n.

(vii) Demonstrate that the edge arrow and vertex key matching rules are equivalent to the requirements of continuous, infinite, and straight primary and secondary Ammann lines and that this excludes the possibility of constructing a periodic tiling.

(viii) Demonstrate that any tiling obeying the matching rules at all edges and vertices must be a member of the PLI class.

(ix) Demonstrate the equivalence between the dual of the Ammann quasilattice and the dual of the appropriate periodic N-grid, thereby showing that the tilings defined by deflation are the same as those defined by projection.

The tenfold case has been treated in detail in the literature.[5] In this section only the eightfold and twelvefold cases will be discussed.

B. Derivations and proofs

We begin with two *ansätze* motivated by their simplicity and by the known structure of the Penrose tilings.

A1: The Ammann quasilattice is indeed composed of quasiperiodic grids of the form defined above.

A2: The way to form the unscaled deflation of the Ammann quasilattice is to deflate each grid independently according to the following rule:

$$D1:\quad T=\frac{T^*}{2}S^{*n}\frac{T^*}{2};\quad S=\frac{T^*}{2}S^{*(n-1)}\frac{T^*}{2}\ ,$$

where S^{*n} denotes n S^*'s in a row and $T^*/2$ denotes half of a T^* interval. Figure 8 illustrates this rule. For the twelvefold case, we will see that this ansatz must be modified to

$$D2:\quad T=\frac{T^*}{2}S^{*(n-1)}\frac{T^*}{2};\quad S=\frac{T^*}{2}S^{*n}\frac{T^*}{2}\ .$$

Note that $S>T$ in this case.

We will find, of course, that **A1** and ***A2*** (using $D2$ for

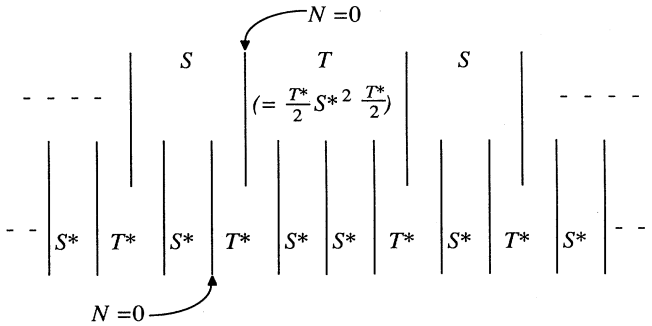

FIG. 8. Unscaled deflation of a single quasiperiodic grid. Rule D1 is illustrated for the case $n=2$.

the twelvefold case) lead to tilings with the desired properties and therefore are sufficient for our purposes.

1. *Deflation of single grids*

de Bruijn has shown[24] that the only sequences of the form of Eq. (11) that can be inflated infinitely many times according to ($D1$) are those with $\sigma=[n+(n^2+4)^{1/2}]/2$ and that the deflation rule for β is

$$\beta^*=\frac{1}{\sigma}(\lfloor\beta\rfloor-\beta)\ . \tag{12}$$

The value of n that is appropriate for Q-fold symmetry is one for which σ turns out to be of the form $m+2l\cos(2\pi/Q)$ for some integers m and l. It can be shown that this is the only choice for which there can exist a minimum separation between intersections of the Q-fold Ammann quasilattice, as must be the case if the Ammann quasilattice is to be obtainable via tile decoration. The tenfold Ammann quasilattice corresponds to the choice $n=1$. For $Q=8$, the appropriate choice is $n=2$, yielding $\sigma=1+\sqrt{2}\equiv\omega$. For $Q=12$, however, we require that σ be $m+l\sqrt{3}$, which cannot be achieved for sequences of the form considered. A slight modification of de Bruijn's analysis reveals that the deflation rule $D2$ with $n=3$ corresponds to a sequence of the form of Eq. (11) with $\sigma=2+\sqrt{3}\equiv\xi$. The deflation rule for β is modified slightly:

$$\beta^*=\frac{1}{\xi}(-\lfloor\beta\rfloor+\beta-1)\ . \tag{13}$$

Note that since S is longer than T, σ' must be negative.

Since the grid itself is of interest here, not just the order of the intervals, we must also consider α and σ'. The value of σ' is determined by the requirement that the ratio $T/S=1+(1/\sigma')$ be invariant under deflation; for the eightfold case,

$$\frac{T^*}{S^*}=\frac{T}{S}=\frac{T^*+2S^*}{T^*+S^*} \tag{14}$$

yields $\sigma'=\omega$; for the twelvefold case,

$$\frac{T^*}{S^*}=\frac{T^*+2S^*}{T^*+3S^*} \tag{15}$$

yields $\sigma'=-\xi$. Inspection of the positions of the $N=0$ line before and after deflation (see Fig. 8) leads to the deflation rule for α:

$$\alpha^*=\sigma\left[\alpha+\frac{1}{\sigma'}\lfloor\beta\rfloor-\frac{1}{2\sigma}\left[1+\frac{1}{\sigma'}\right]\right]-\frac{1}{\sigma'}\lfloor\beta^*\rfloor\ . \tag{16}$$

Here, α^* has been scaled so that it corresponds to the rescaled deflation, in which the interval lengths are the same as those in the original grid.

2. *The $\{\alpha_n,\beta_n\}$ of the PLI class*

The $\{\alpha_n,\beta_n\}$ that produce Ammann quasilattices (quasiperiodic N-grids in the PLI class) can be found by applying the condition that $\{\alpha_n^*,\beta_n^*\}$ is locally congruent to $\{\alpha_n,\beta_n\}$. The analysis leading to Eq. (5) is closely analogous to the treatment of the tenfold case in Ref. 5. For completeness, the modified analysis for the eightfold and twelvefold cases is given in the appendixes. In Appendix A, it is shown that all locally congruent $\{\alpha_n,\beta_n\}$ can be written in the form

$$\begin{aligned}\alpha_n&=\alpha_n+\mathbf{u}\cdot\mathbf{e}_n+p_n+\frac{1}{\sigma'}q_n\ ,\\ \beta_n&=b_n+\mathbf{w}\cdot\mathbf{e}_\pi-q_n+\frac{1}{\sigma}p_n\ ,\end{aligned} \tag{17}$$

where a_n and b_n are specified constants, $\mathbf{u}$ and $\mathbf{w}$ are arbitrary vectors, and p_n and q_n are arbitrary integers. In Appendix B, the local congruence of the deflated quasilattice and its parent is shown to lead to the values of a_n and b_n quoted in Eq. (5).

3. *The secondary Ammann quasilattice decoration*

Given the PLI class tiling, we can attempt to find a decoration that produces continuous straight lines normal to the $\mathbf{e}_n+\mathbf{e}_{n+1}$ directions. The decoration shown in Fig. 4 is the result of some guesswork guided by the goal of producing appropriate spacings between parallel lines. To see that this decoration can be consistently applied to produce infinite lines in the tiling, one need only check the properties of the decoration under deflation. Beginning with a single tile of any shape and performing enough deflations to ensure that all the allowed nearest-neighbor configurations are deflated at least once, one finds that the decoration of the deflated tiles always consists of continuous, straight lines. Since the deflation of the tiles around an allowed vertex is unique, repeated deflation must always yield continuous lines. Furthermore, the behavior of the decoration lines under deflation is given precisely by the rule for deflation of the Ammann quasilattice. The new decoration is therefore called the "secondary Ammann quasilattice."

An important aspect of the secondary Ammann quasilattice decoration is that it breaks the mirror symmetries of the primary Ammann quasilattice decoration. It is found that the different ways in which the tiles are decorated by the primary and secondary Ammann quasilattices distinguish tile orientations in a manner equivalent to the arrows marking the tiles in Fig. 1. Note

that the primary Ammann-line decoration is not sufficient for fully determining the orientation of every marked tile, in the following sense: For an arbitrarily large, but finite distance, d, even if the examination of regions of radius d surrounding each tile is permitted, there will be an infinite number of tiles whose proper orientations cannot be determined. This point will be clarified in Sec. IV, where special configurations will be identified in which tile orientations can be flipped without any consequent alteration of the primary Ammann lines.

4. *The $\{\alpha_{nm},\beta_{nm}\}$ of the secondary Ammann quasilattice*

Since the secondary Ammann quasilattice is deflated according to the same rule as the primary Ammann quasilattice, it can be specified by equations similar to Eqs. (4) and (5). It is clear that $\mathbf{f}_{nm}$ [see Eq. (8) and Fig. 3] plays the role of $\mathbf{e}_n$ on the left-hand side. All that remains is to determine the values of α_{nm} and β_{nm} in Eq. (10).

There are two eightfold tilings that have a center of eightfold symmetry (in a sense that will soon be made explicit): the "star" pattern and the "cartwheel" pattern. (The names derive from analogous patterns in Penrose tilings.[7]) In the star pattern, both the undecorated tiles and the primary Ammann quasilattice are invariant under rotations by $2\pi/8$ about a central point. The tiles sharing the central vertex form a star of eight rhombi. The center of the cartwheel pattern is depicted in Fig. 9. It is completely invariant under rotation by $2\pi/8$ except for the tiles in the central octagon and those that are shaded in the figure (the tiles intersected by sixteen rays emanating from the center). The cartwheel pattern is said to have a center of symmetry because the set of shaded tiles has measure zero in the set of all tiles in the pattern and the diffraction pattern, including phases, has perfect C_{8v} symmetry. Similarly, there is a cartwheel pattern in the twelvefold case whose diffraction pattern has perfect C_{12v} symmetry. The twelvefold cartwheel tiling has perfect C_{12v} symmetry outside of a central dodecagon and 24 rays of tiles emanating from it.

The $\{\alpha_n,\beta_n\}$ for the cartwheel pattern can be found using the fact that there exist infinitesimal shifts in $\mathbf{w}$ that affect only the lines passing closest to the center of symmetry (one in each grid). If these lines are taken to have index $N=0$, then β_n must differ only by an infinitesimal amount from some integer. Umklapp equivalence (see Appendix A) allows this integer to be chosen to be zero. Thus $\beta_n^{\text{cartwheel}}=\delta\mathbf{w}\cdot\bar{\mathbf{e}}_n=0^{\pm}$, where $\delta\mathbf{w}$ is infinitesimal. From simple geometry and the primary Ammann quasilattice decoration applied to Fig. 9, it can be determined that $\alpha_n^{\text{cartwheel}}=1/(2\sigma')$ for all n. Applying the secondary Ammann quasilattice decoration to the cartwheel pattern reveals that it is also a cartwheel Ammann quasilattice, implying that $\beta_{nm}^{\text{cartwheel}}=0^{\pm}$ and $\alpha_{nm}^{\text{cartwheel}}=1/(2\sigma')$. (Since the tiling has a center of eightfold symmetry, the secondary Ammann quasilattice had to be either a star or a cartwheel. It is amusing to note that the secondary Ammann quasilattice for the star pattern is also a cartwheel Ammann quasilattice, as could be surmised from the observation that the matching rule decoration breaks the symmetry of the central star.)

Now the effect of a translation by $\mathbf{u}$ on α_n is simply given by $\Delta\alpha_n=\mathbf{u}\cdot\mathbf{e}_n$. Similarly, one has $\Delta\alpha_{nm}=\mathbf{u}\cdot\mathbf{f}_{nm}=\mathbf{u}\cdot(\mathbf{e}_n+\mathbf{e}_m)=\Delta\alpha_n+\Delta\alpha_m$. Consideration of β translations (see Appendix A) establishes that $\bar{\mathbf{f}}_{nm}\equiv\bar{\mathbf{e}}_n+\bar{\mathbf{e}}_m$ plays the role of $\bar{\mathbf{e}}_n$ in Eq. (5) and $\Delta\beta_{nm}=\Delta\beta_n+\Delta\beta_m$. Combining these relations with the known cartwheel values immediately yields

$$\alpha_{nm}=\alpha_n+\alpha_m-\frac{1}{2\sigma'},\quad \beta_{nm}=\beta_n+\beta_m\ . \tag{18}$$

5. *Matching rules, nonperiodicity, and quasiperiodicity*

It is obvious by inspection of Fig. 2 that enforcing the edge arrow rules is equivalent to requiring that the primary Ammann lines be continuous, straight, and infinite. The vertex key rules and the continuity of the secondary Ammann quasilattice are not completely equivalent, but the following can be established by exhaustive checking of relevant configurations: Regardless of whether the edge arrow rules are obeyed, if the secondary Ammann lines are continuous over a set of tiles, then the vertex key rules are obeyed at all vertices surrounded by that set. Thus, enforcing the continuity of the secondary Ammann lines guarantees that the vertex key rules will be satisfied. Furthermore, *if the edge arrow rules are obeyed,* then enforcing the vertex key rule guarantees that the secondary Ammann lines will be continuous. To prove these assertions, it is sufficient to examine all possible neighborhoods consisting of a single tile and the ones that share at least one vertex with it.

The mere fact that the Ammann lines are straight and continuous is sufficient to ensure that no periodic structure is compatible with the matching rules. It is easy to see by placing just a few tiles consistent with the matching rules that at least one line in each of the orientations of the primary and secondary grids must appear in the tiling. (In fact, every allowed neighborhood containing a single tile and all those sharing a vertex with it contain Ammann lines in all of the directions.) We will show that it is impossible to form a periodic structure that incorporates continuous lines in all of the Ammann-line directions with a nonzero minimum spacing between parallel Ammann lines (an obvious property of the Ammann quasilattice decorations).

The following proof relies only on simple geometry: Assume a periodic (crystalline) structure exists that contains infinite lines making angles of $n\theta$ with the x axis, where $\theta=2\pi/Q$ and $n=0,1,\ldots,Q/2$. Let $\mathbf{b}_1'$ and $\mathbf{b}_2'$, with polar coordinates (r_1',ϕ_1') and (r_2',ϕ_2'), be the basis vectors of the unit cell of the structure. The simultaneous requirements that the lines be continuous at the unit cell borders and that there be a minimum spacing between parallel lines place a constraint on the values of r_i' and ϕ_i'. In Fig. 10, $x/\|\mathbf{b}_2'\|=x/r_2'$ must be rational, implying

$$\frac{r_1'\sin(n\theta-\phi_1')}{r_2'\sin(n\theta-\phi_2')}=\frac{p_n}{q_n}\ , \tag{19}$$

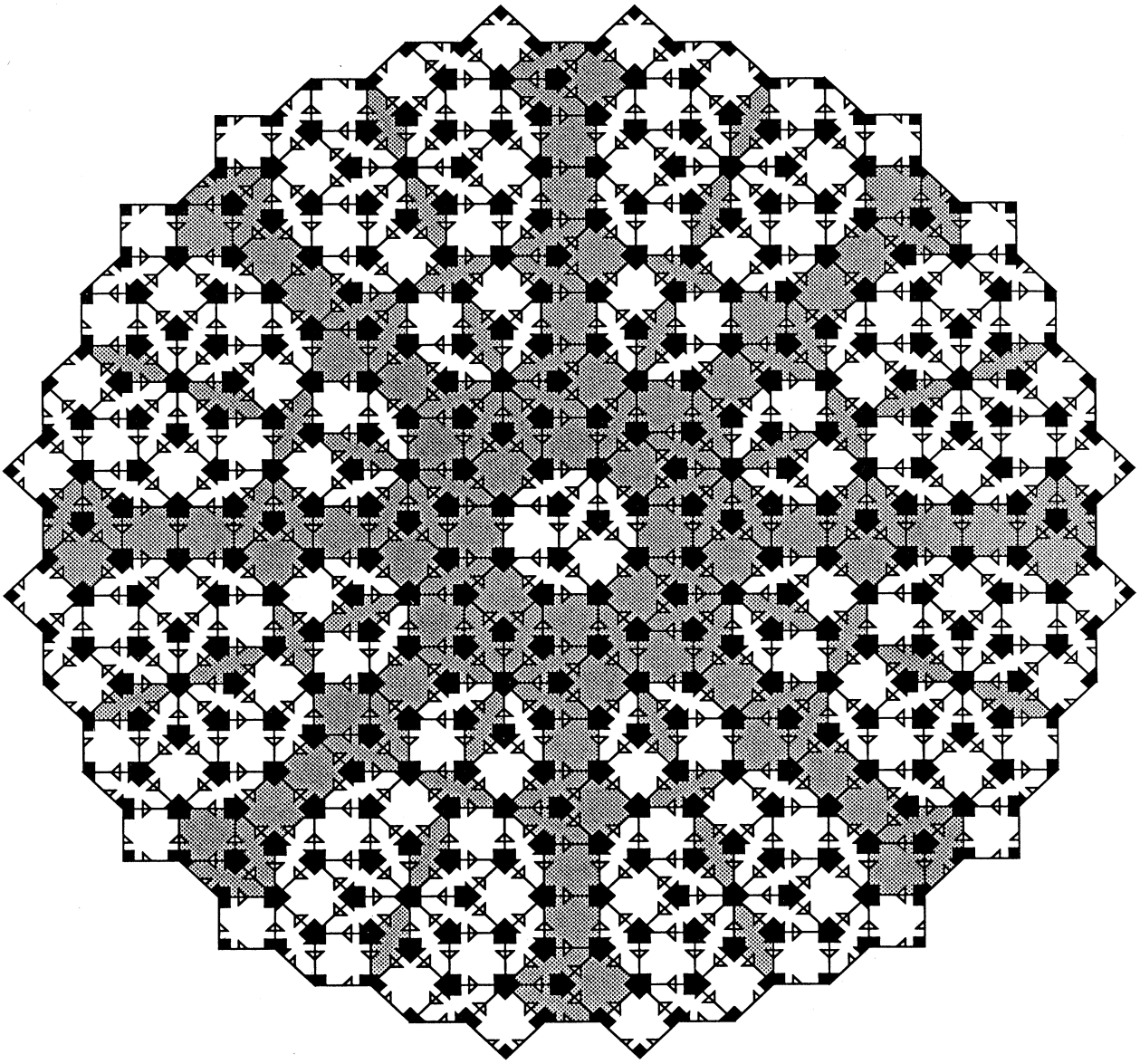

FIG. 9. Center of the octagonal cartwheel pattern. Outside of the sixteen rays of shaded tiles and the central octagon, this pattern has perfect C_{8v} symmetry. The ray of shaded tiles comprises a semi-infinite primary or secondary worm. (See text, Sec. IV A, and compare Fig. 11.)

where p_n and q_n are integers. Without loss of generality, a new unit cell can be chosen with basis vectors $\mathbf{b}_1 = q_0\mathbf{b}_1' - p_0\mathbf{b}_2'$ and $\mathbf{b}_2 = q_1\mathbf{b}_1' - p_1\mathbf{b}_2'$. Simple geometry shows that $\mathbf{b}_1$ and $\mathbf{b}_2$ can be written as $(r_1,0)$ and (r_2,θ), respectively. With this choice of basis vectors, the continuity and minimum separation condition becomes

$$\frac{r_1\sin(n\theta)}{r_2\sin[(n-1)\theta]} = \frac{p_n}{q_n}, \quad \forall n \neq 1 . \tag{20}$$

For $n=2$, the condition reduces to $(r_1/r_2)2\cos\theta = p_2/q_2$; for $n=3$ we get $(r_1/r_2)\cos\theta(2-\frac{1}{2}\sec^2\theta) = p_3/q_3$. Combining these we find a necessary condition on θ:

$$\cos^2\theta = \left[4 - \frac{4p_3q_2}{p_2q_3}\right]^{-1} = \text{a rational number} . \tag{21}$$

The only values of $\theta = 2\pi/Q$ that satisfy the condition are $\theta = \pi$, $\pi/2$, $\pi/3$, $\pi/4$, and $\pi/6$. Now including both primary and secondary Ammann lines in the case of Q-fold symmetry corresponds to $\theta = \pi/Q$. Thus continuous primary and secondary Ammann lines are incompatible with periodicity for $Q = 8$, 10, or 12. This completes the proof.

Note that if the primary Ammann lines alone are con-

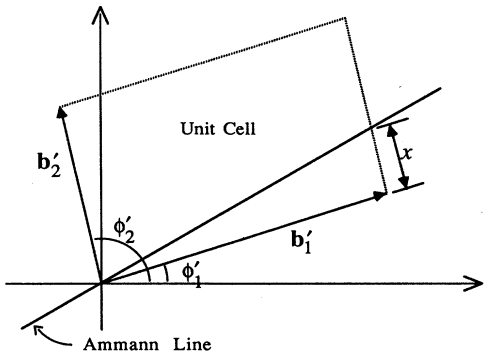

FIG. 10. Aid for proof of nonperiodicity (Sec. III B 5). A unit cell of a periodic structure is shown with an Ammann line running through it. If the Ammann lines are to be continuous and parallel ones are to be separated by a minimum distance, then $x/\|\mathbf{b}_2'\|$ must be rational.

sidered, the relevant value of θ is $2\pi/Q$. For $Q=10$, periodicity is still ruled out, but not for $Q=8$ or 12. We will see, in Sec. IV, that it is indeed possible to construct periodic tilings using the eightfold or twelvefold tiles with only primary Ammann line (or edge arrow) matching rule constraints. For these cases, the secondary Ammann lines (or the vertex keys) are essential for the exclusion of periodic tilings.

The preceding proof has the virtue of being easily understandable, but does not establish the fact that the matching rules actually restrict the infinite tiling to be quasiperiodic and a member of a particular LI class. We now show that any infinite tiling obeying the matching rules is indeed a member of the PLI class by demonstrating that it can be repeatedly inflated *ad infinitum* according to the rules depicted in Fig. 1. Recall that the condition of repeated inflatability was the basis of the proof of quasiperiodicity of the Ammann grids (Sec. III B 1). Furthermore, since local isomorphism under deflation is guaranteed by the repeated inflatability condition, the values of $\{\alpha_n,\beta_n\}$ are also determined. To establish the property of repeated inflatability, we will show first that any tiling obeying the matching rules can be inflated *once,* and next that the inflated tiles also obey the matching rules.

To see that any tiling can be inflated once, it is sufficient to consider the local configurations around individual tiles. Let **O** denote a single tile in an infinite pattern where the matching rules are everywhere satisfied, let **I** denote the (unscaled) inflated tile or set of tiles that include all or part of **O**, and let **D** denote the set of tiles in the original tiling that overlap at least one tile in **I**. (One of the tiles in **D** is **O**.) We must show that **I** always exists, that **O** is completely covered by **I**, and that **I** is uniquely determined by **D**. Under such conditions, it can be concluded that every tile in the original pattern is included in inflated tiles in exactly one way and therefore that the entire inflation can be consistently pieced together from the inflations of local regions. To show that **I** always exists, we need only construct all possible neighborhoods of a given tile **O** that are consistent with the matching rules and check them to see that **O** can indeed be covered by some **I**. These same neighborhoods can also be checked to see that **D** determines **I** uniquely.

In contrasting the possible neighborhoods, it is useful to classify tiles that can be added to a given cluster as "forced" or "unforced." Consider a finite cluster of tiles and the possible ways of adding a tile to it. At certain edges on the perimeter of the cluster the matching rules may leave no choice as to the type of tile that must be added or its orientation. The tile that must be added at such an edge is called "forced." At other (unforced) edges, there may be several possible choices of tiles to add, all consistent with the matching rules.

An efficient way to generate the complete list of neighborhoods is as follows: Begin with a single tile and choose an edge where a new (unforced) tile will be added. Label the possible choices consistent with the matching rules $1_1, 1_2, \ldots, 1_n$. Add choice 1_1 to the original tile and fill in all tiles that are forced by this choice. Now choose an edge on the perimeter of the cluster and label the possible additions there $2_1, 2_2, \ldots$. Do the same for tiles 1_2 through 1_n. Continuing this procedure in the obvious way generates all possible neighborhoods of the original tile, each specified by the labels of the choices made in generating it. (Note that a "2_i" following a "1_j" may correspond to a different tile than does a "2_i" following a "1_k".) Each sequence of choices $(1_i, 2_j, 3_k, \ldots)$ need only be extended to the point where the inflated tiles in a set (**I**) that completely covers the original **O** are themselves completely covered by the smaller tiles (**D**), so the number of sequences that must be checked is finite. In addition, that number can be minimized by symmetry considerations, judicious choices of unforced edges at which tiles are added, and some observations relevant to the particular tiling in question. For example, for the matching rules of the eightfold tiling, it is not necessary to check the neighborhoods of the 45° rhombus. In checking the neighborhoods of the square, one sees that any 45° rhombus sharing an edge with a square is already included in the inflation that covers that square and it is easy to check that every 45° rhombus must share an edge with a square. For the twelvefold case, it is sufficient to check the neighborhoods of the hexagon and one neighborhood of the 30° rhombus (the one that occurs in the middle of an inflated 30° rhombus). The procedure of checking all relevant neighborhoods for consistency with inflation has been carried out in full for the eightfold and twelvefold PLI class matching rules using a system for which no sequence longer than five choices was necessary and all choices after the first in each sequence involved only two alternatives.[25]

It is a bit easier to see that the inflated tiles must obey the matching rules. With regard to the edge arrow rules, one need only note that the orientations of the edges of the inflated tiles are unambiguously determined by the position of the deflated square tile along the edge in the eightfold case and the orientation of the deflated hexagon on the edge in the twelvefold case—the two inflated tiles sharing an edge obviously must match along it. The following observations make it clear that the vertex key rules are also obeyed. Each vertex in the inflated tiling coincides with a vertex in the original tiling. We now

compare the section of the original vertex key that is covered by a single inflated tile with the section of the inflated vertex key contributed by the same inflated tile. In the twelve-fold case, inspection of the deflated decoration immediately reveals that these two sections are identical in shape and orientation. Thus the shape and orientation of the key occurring at any vertex shared by the original and inflated tiling are guaranteed to be preserved under inflation; the vertex key rule is obeyed in the inflation if it is obeyed in the original. In the eightfold case, the same result holds, but the reasoning involves a surprising twist. Consider each vertex key to be divided into eight sections as shown in Fig. 5(c). When a given vertex is deflated or inflated, the orientation of each section of the key is reversed, as can be seen by inspection of the deflation decoration. (Each section is reflected about the bisector of its angle at the vertex.) Note, however, that when all the sections are flipped in this manner, a new vertex key is formed which has the correct form (!), though its orientation is opposite to the original.

These results establish rigorously the fact that any infinite tiling that is everywhere consistent with the matching rules of Fig. 5 is a member of the PLI class. It must be emphasized, however, that a *finite* portion of a tiling may be inconsistent with the PLI class tilings, even if it does not contain a matching rule violation, as is well known for the decagonal case. Such a configuration will support only a finite number of inflations before a matching rule violation occurs. Let r be the radius of the original configuration and n be the number of inflations that can be carried out. It is straightforward to show that it is impossible to extend the configuration to cover a circle of radius $r\sigma^{n+1}$ centered on the original cluster, where σ is the inflation scale factor.

6. *Duals of Ammann quasilattice and periodic ($Q/2$) grid are in same LI class*

To establish the isomorphism between the tilings defined by the dual of the primary Ammann quasilattice and those produced by projection, it is sufficient to show that one particular Ammann quasilattice dual is equivalent to one particular projected tiling. The most convenient choice is the cartwheel tiling, which, as will be demonstrated, is identical to the dual of the periodic $Q/2$-grid with $\gamma_n=0$ for all n. The proof is given here for the eightfold case; a similar procedure establishes the same result for the twelvefold case.

Recall that the Ammann quasilattice of the cartwheel tiling has complete eightfold symmetry outside of the $N=0$ lines (those passing to the center of symmetry). The $N=0$ lines are "singular" in the sense that their position can shift for infinitesimal shifts in $\mathbf{w}$, since $\beta_n=0$. Similarly, the periodic 4-grid with $\gamma_n=0$ for all n is singular in the sense defined in Ref. 10; the grid intersections containing $N=0$ lines are all points at which more than two lines intersect. In the following proof, the tiles dual to these singular intersections will be ignored. It is straightforward to show that the singularities can be resolved in the same way for the Ammann quasilattice and the periodic 4-grid.

To show that the two dual tilings are the same, it suffices to verify that the square tiles in them occur in identical positions. In the dual construction, the position of the tile vertex dual to a given open region in the 4-grid is given by $\sum_n k_n\mathbf{e}_n$, where the open region lies between grid lines of index k_n and k_n+1 for all n. The vertices of a square tile dual to the intersection of line M in grid $\mathbf{e}_0$ and line N in grid $\mathbf{e}_2$ occur at the points $(M-i)\mathbf{e}_0+(N-j)\mathbf{e}_0+k_1\mathbf{e}_1+k_3\mathbf{e}_3$, where $i=0,1$ and $j=0,1$. We will show that $k_1^{(\mathrm{Aql})}$ and $k_1^{(\mathrm{Proj})}$, the values obtained for k_1 from the Ammann quasilattice and the periodic 4-grid, are identical. The octagonal symmetry of both the Ammann quasilattice and the 4-grid then implies that both yield the same value of k_3 as well and that similar identities hold for square tiles in the other orientations.

It is easy to compute $k_1^{(\mathrm{Proj})}$: In the singular periodic 4-grid, an intersection point $\mathbf{x}$ dual to a square is determined by $\mathbf{x}\cdot\mathbf{e}_0=M$, $\mathbf{x}\cdot\mathbf{e}_2=N$. By definition, $k_1^{(\mathrm{Proj})}$ is equal to $\lfloor\mathbf{x}\cdot\mathbf{e}_1\rfloor$, which is equal to $\lfloor 1/\sqrt{2}(M+N)\rfloor$. For the cartwheel Ammann quasilattice, on the other hand, we have

$$\mathbf{x}\cdot\mathbf{e}_0=M+\frac{1}{2\omega}+\frac{1}{\omega}\left\lfloor\frac{M}{\omega}\right\rfloor,$$

$$\mathbf{x}\cdot\mathbf{e}_2=N+\frac{1}{2\omega}+\frac{1}{\omega}\left\lfloor\frac{N}{\omega}\right\rfloor, \tag{22}$$

$$\Longrightarrow \mathbf{x}\cdot\mathbf{e}_1=\frac{N+M}{\sqrt{2}}+\frac{1}{\sqrt{2}\omega}+\frac{1}{\sqrt{2}\omega}\left\lfloor\left\lfloor\frac{M}{\omega}\right\rfloor+\left\lfloor\frac{N}{\omega}\right\rfloor\right\rfloor,$$

and $k_1^{(\mathrm{Aql})}$ is defined as the value of k for which

$$k+\frac{1}{2\omega}+\frac{1}{\omega}\left\lfloor\frac{k}{\omega}\right\rfloor<\mathbf{x}\cdot\mathbf{e}_1<k+1+\frac{1}{2\omega}+\frac{1}{\omega}\left\lfloor\frac{k+1}{\omega}\right\rfloor. \tag{23}$$

These inequalities can now be directly verified for $k=k_1^{(\mathrm{Proj})}$. Consider first the left inequality. We want to show that

$$\mathbf{x}\cdot\mathbf{e}_1-k_1^{(\mathrm{Proj})}-\frac{1}{2\omega}-\frac{1}{\omega}\left\lfloor\frac{k_1^{(\mathrm{Proj})}}{\omega}\right\rfloor>0. \tag{24}$$

Substituting the above expressions for $\mathbf{x}\cdot\mathbf{e}_1$ and $k_1^{(\mathrm{Proj})}$, we have for the left-hand side of Eq. (24),

$$z+\frac{1-\sqrt{2}}{2\omega}+\frac{1}{\sqrt{2}\omega}\left\lfloor\left\lfloor\frac{M}{\omega}\right\rfloor+\left\lfloor\frac{N}{\omega}\right\rfloor\right\rfloor-\lfloor z\rfloor-\frac{1}{\omega}\left\lfloor\frac{\lfloor z\rfloor}{\omega}\right\rfloor, \tag{25}$$

where $z\equiv(1/\sqrt{2})(M+N)$. Let $\{x\}$ denote the fractional part of x. The identities $x=\lfloor x\rfloor+\{x\}$ and $\{x+y\}=\{x\}+\{y\}-\lfloor\{x\}+\{y\}\rfloor$ can be used repeatedly to reduce Eq. (25) to

$$\frac{1}{2\omega}+\frac{1}{\sqrt{2}\omega}\left[2\{x\}-\{2z\}+1-\left\lfloor\left\{\frac{M}{\omega}\right\}+\left\{\frac{N}{\omega}\right\}\right\rfloor\right]+\frac{1}{\omega}\lfloor\sqrt{2}\{z\}\rfloor. \tag{26}$$

The identity $2\{x/2\}-\{x\}=\lfloor x\rfloor \pmod 2$ allows the final result

$$\frac{1}{2\omega}+\frac{1}{\sqrt{2}\omega}\left[1+[\lfloor z\rfloor \pmod 2]-\left|\left\{\frac{M}{\omega}\right\}+\left\{\frac{N}{\omega}\right\}\right|\right]+\frac{1}{\omega}\lfloor\sqrt{2}\{z\}\rfloor\ . \quad (27)$$

Since $0\le\{x\}<1$, Eq. (27) can take on only the values $1/\omega(\frac{1}{2}+p/2+q)$, with $p=0,1,2$ and $q=0,1$, and Eq. (24) is satisfied. The inequality on the right in Eq. (23) can be established in a similar fashion, or it can be inferred immediately from the left inequality and the symmetry of the Ammann quasilattice under rotation by π.

We have demonstrated the equivalence of the duals to the Ammann quasilattice with $\alpha_n=1/(2\omega)$, $\beta=0$, and the projected tilings with $\gamma_n=0$ and thereby shown that the Ammann quasilattice duals and the projected tilings belong to the same LI class.

7. *Calculation of tile frequencies*

As a check of the last result, we compute the ratios of the frequencies of occurrence of the various tile types in two different ways. First, the ratios implied by the deflation rules are calculated: Let the number of each type of tile be denoted by R_f (fat rhombus in tenfold), R_s (skinny in tenfold), R_s (rhombus in eightfold), S_8 (square in eightfold), R_{12} (rhombus in twelvefold), S_{12} (square in twelvefold), and H_{12} (hexagon in twelvefold), and let a superscript "$*$" denote values in the once-deflated tiling. Substitution matrices, $\underline{M}_N$, are defined by

$$\begin{bmatrix}R_f^*\\R_s^*\end{bmatrix}=\underline{M}_{10}\begin{bmatrix}R_f\\R_s\end{bmatrix},\quad \begin{bmatrix}S_8^*\\R_8^*\end{bmatrix}=\underline{M}_8\begin{bmatrix}S_8\\R_8\end{bmatrix},\quad \begin{bmatrix}H_{12}^*\\S_{12}^*\\R_{12}^*\end{bmatrix}=\underline{M}_{12}\begin{bmatrix}H_{12}\\S_{12}\\R_{12}\end{bmatrix}. \quad (28)$$

The ratio of tile frequencies after an infinite number of deflations is given by the eigenvector corresponding to the maximal eigenvalue of $\underline{M}_N$. Inspection of Fig. 1 immediately establishes

$$\underline{M}_{10}=\begin{bmatrix}2&1\\1&1\end{bmatrix},\quad \underline{M}_8=\begin{bmatrix}3&2\\4&3\end{bmatrix},\quad \underline{M}_{12}=\begin{bmatrix}7&2+x&2-x\\12&1+y&6-y\\12&4&3\end{bmatrix}, \quad (29)$$

where $x=(3+5\sqrt{3})/9$ and $y=4\sqrt{3}/3$. For the infinite tilings, one obtains

$$R_f{:}R_s=\tau{:}1,\quad S_8{:}R_8=1{:}\sqrt{2}\ ,\quad H_{12}{:}S_{12}{:}R_{12}=1{:}\sqrt{3}{:}\sqrt{3}\ . \quad (30)$$

A straightforward extension treating mirror-image partners as distinct confirms that in every case they occur with the same frequency.

Next, we compute the frequency ratios implied by the GDM applied to periodic $(Q/2)$-grids: All the tiles of a given type and orientation are dual to the intersections of the lines in two particular grids. The density of the intersections of two grids is simply given by $\sin\theta$, where θ is the angle between the vectors normal to the grids. The frequency of occurrence of a rhombic tile having an acute angle θ is therefore given by $\sin\theta$ times the number of ways two grids can be chosen such that the acute angle formed by the intersecting lines is θ. Thus, for example, the frequencies of occurrence of the 45° rhombus and the square in the eightfold case are $4\sin(\pi/4)$ and $2\sin(\pi/2)$, respectively, in agreement with the deflation result. The density of hexagons in the twelvefold tiling is obtained by computing the density of 60° intersections and dividing by three, since each hexagon can be composed from three 60° rhombi. The other cases are all straightforward and agree with Eq. (30).

IV. IRREDUCIBLE PHASON STRAINS

The canonical methods of elasticity theory can be applied in a straightforward way to quasicrystals.[18,21,26] For eightfold, tenfold, and twelvefold quasicrystals, the 2D vectors $\mathbf{u}$ and $\mathbf{w}$ of Eq. (5) are associated with continuous symmetries that are spontaneously broken in the perfectly ordered state. Uniform shifts in $\mathbf{u}$ merely translate the entire system, so a particular choice of $\mathbf{u}$ breaks the continuous translational symmetry of the free energy. Similarly, uniform shifts in $\mathbf{w}$ produce different members of the same LI class, and a choice of $\mathbf{w}$ is said to break the continuous phason symmetry of the free energy. Elastic distortions of the quasicrystal are slow spatial variations of $\mathbf{u}$ and $\mathbf{w}$ and, in the long-wavelength limit, are the deformations of lowest energy.

A given linear elastic distortion, or uniform strain, is specified by $\partial_i\mathbf{u}_j=\mu\mathbf{M}_{ij}^{(u)}$ (the conventional strain tensor) or $\partial_i\mathbf{w}_j=\nu\mathbf{M}_{ij}^{(w)}$ (the phason strain tensor), where i and j index the two spatial dimensions, μ and ν are positive constants that determine the magnitude of the strain, and $\mathbf{M}$ is normalized such that $\mathbf{M}_{ij}\mathbf{M}_{ij}=1$. For a uniform phason strain, we have $\mathbf{w}_j=\mathbf{x}_i\nu\mathbf{M}_{ij}^{(w)}$ or $\mathbf{w}=\mathbf{x}\cdot\nu\mathbf{M}^{(w)}$. The set of all $\mathbf{M}^{(w)}$ can be spanned by a set of basis elements whose members transform among each other under an irreducible representation of the orientational symmetry group of the quasicrystal. A strain tensor that can be formed as a linear combination of the basis elements corresponding to a single irreducible representation is called an irreducible strain. Familiar examples of irreducible strains are the compressions and shears of an isotropic solid. The strain tensor corresponding to compression, for instance, is a multiple of the identity matrix and transforms under the scalar representation of the symmetry group O(2).

In this section, the number and form of the irreducible strains is derived for quasicrystals with eightfold, tenfold, and twelvefold symmetry. We begin, in Sec. IV A, with a preliminary discussion of the signature of phason strain in the PLI class tilings. Phason strain induces isolated matching rule violations in a tiling which correspond to certain discontinuities induced in the Ammann quasilattice. In Sec. IV B, the irreducible strains are derived and some of their distinguishing features are presented. In the eightfold and twelvefold cases, there exist irreducible phason strains that induce discontinuities in only the primary Ammann quasilattice, and others that induce discontinuities in the secondary Ammann quasilattice. In the tenfold case, all phason strains induce discontinuities in the primary Ammann quasilattice (which is why the secondary Ammann quasilattice has not been treated in this paper for the tenfold case).

A. Phason strains in the PLI class tilings

The determination of the tiling configurations associated with phason strain is made on the basis of the GDM applied to strained Ammann quasilattices. Since $\mathbf{w}$ appears in Eqs. (4) [with β_n defined in Eq. (5)] only within the greatest integer function, smooth spatial variations in $\mathbf{w}$ produce discontinuous "jags" in the Ammann lines. (The distribution of jags associated with different types of phason strain is discussed in the next section.) Jags correspond to particular kinds of isolated matching rule violations in the tilings. Figure 11 illustrates the matching rule violations associated with variations in $\mathbf{w}$ in the eightfold and twelvefold tilings. (The tenfold case is treated in Ref. 18.) Each panel of the figure shows the region surrounding a single jag in one Ammann line. Panels (a) and (b) each show a jag in a primary Ammann

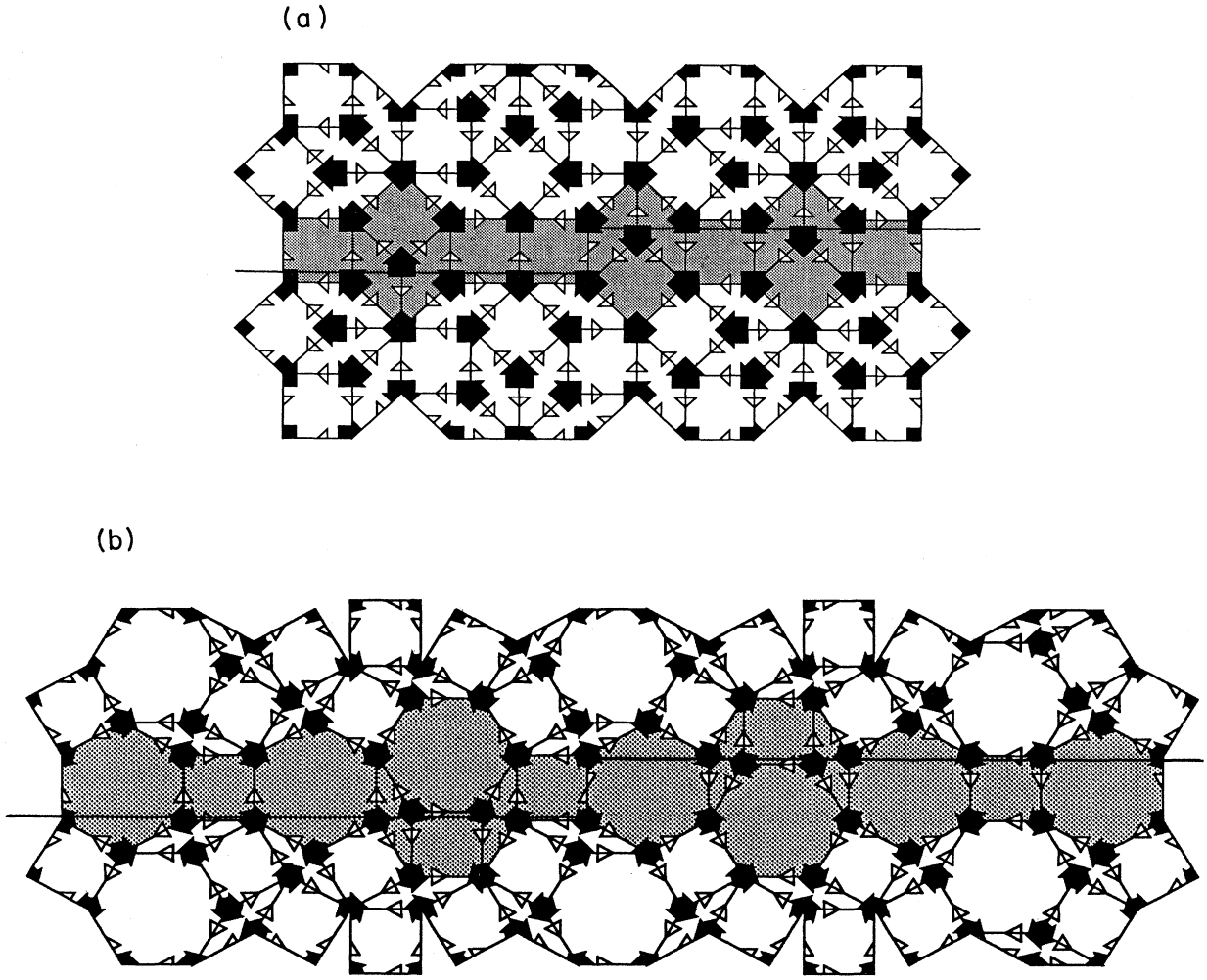

FIG. 11. Primary and secondary matching rule violations. The two line segments shown extending from the shaded tiles lie on the Ammann line that contains a jag. (a), (b) Primary mismatches in the eightfold and twelvefold PLI class tilings. The shaded tiles form a single worm, but the right side of the worm has been flipped with respect to the left, leaving a single edge (in the middle of each picture) where the edge arrow directions do not match. (c), (d) Secondary mismatches in the eightfold and twelvefold PLI class tilings. In the case of a secondary worm, flipping one of its halves with respect to the other produces an illegal key at one vertex.

line. The shaded tiles comprise a primary "worm segment." Note that the matching rule decorations on the tiles bordering the worm segment do not determine the orientation of the worm segment; i.e., the worm segment could be reflected through its horizontal axis without violating any matching rules. The jag in the Ammann line divides the worm segment into two pieces, each of which is consistent with the surrounding tiles. The two pieces are "flipped" with respect to each other, however, so that a matching rule violation occurs at the edge where they meet.

It can be shown that for phason strains of small enough magnitude so that the jags are separated by at least several tile lengths, the jags in the primary Ammann quasilattice always occur along worm segments such as the ones shown in the figure. Thus, jags in primary Ammann lines are always associated with violations of the edge-arrow matching rules in the tiling.

Panels (c) and (d) show a jag in a secondary Ammann line. The shaded tiles form a secondary worm segment. The situation is exactly the same as for the primary Ammann-line jag, except that a jag in the secondary Ammann quasilattice appears as a single violation of a vertex key matching rule, rather than an edge-arrow mismatch.

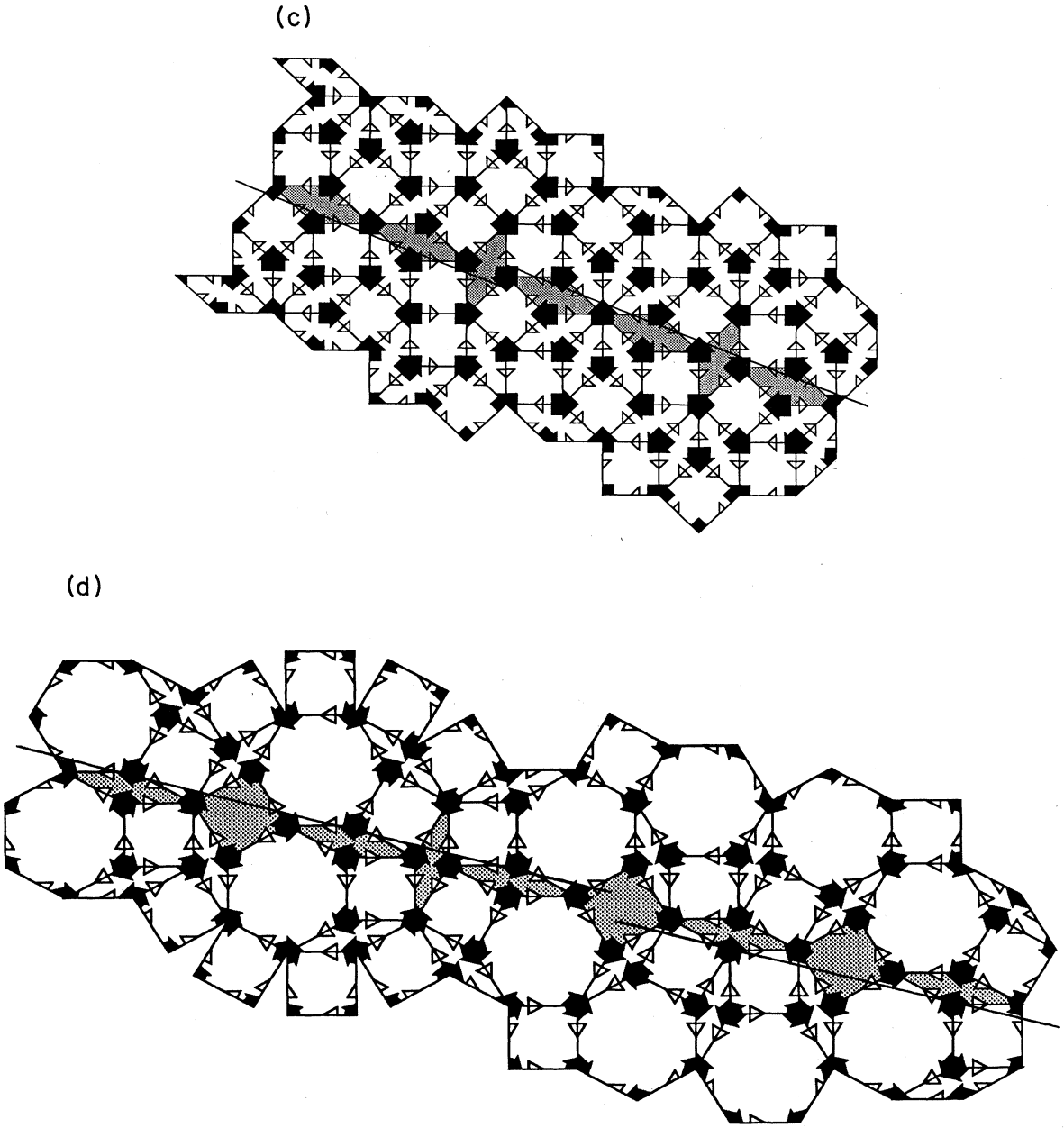

FIG. 11. (*Continued*).

B. Irreducible strains

The transformation properties of $\mathbf{M}^{(u)}$ and $\mathbf{M}^{(w)}$ can be derived from the transformation properties of ∂, $\mathbf{u}$, and $\mathbf{w}$ and some elementary group theory.[27] The gradient operator ∂ and the displacement field $\mathbf{u}$ clearly transform under the ordinary vector representation of the orientational symmetry group. This representation will be denoted by Γ^2. The way in which $\mathbf{w}$ transforms is determined by the requirement that any $\mathbf{w}$ that corresponds to a β translation (which is equivalent to some $\mathbf{u}$) is transformed such that the new $\mathbf{w}$ corresponds to the transformed β translation (i.e., the ordinary vector representation acting on $\mathbf{u}$). (The details of the derivation in each symmetry are left to the reader.) The representation that acts on $\mathbf{w}$ will be denoted $\Gamma^{\bar{2}}$.

In the discussion of phason strains, it is useful to represent the phason strain tensor as a linear combination of dyadics:

$$\mathbf{M}^{(w)}_{ij}=\sum_{n,m} c_{nm}(\mathbf{e}_n)_i(\bar{\mathbf{e}}_m)_j \ , \tag{31}$$

where c_{nm} is a real coefficient. With this notation, the transformation of $M^{(w)}$ under a point-group operation is easily obtained. The $\bar{\mathbf{e}}$'s have been chosen such that if $\mathbf{e}_k$ is transformed into $\mathbf{e}_l$ by the ordinary vector representation of a given operation, then $\bar{\mathbf{e}}_k$ is transformed into $\bar{\mathbf{e}}_l$ under the same operation in $\Gamma^{\bar{2}}$. These transformation rules can be applied independently to the vectors composing $\mathbf{M}^{(w)}$. For example, under rotation by $\pi/6$ in the twelvefold case, $\mathbf{e}_0$ goes to $\mathbf{e}_1$ and $\mathbf{e}_1$ goes to $-\mathbf{e}_2$, so $\mathbf{e}_0\bar{\mathbf{e}}_1$ goes to $-\mathbf{e}_1\bar{\mathbf{e}}_2$.

The orientational symmetry groups of interest here are the groups C_{8v}, C_{10v}, and C_{12v}. The group C_{Qv} (for even Q) has $N=2Q$ elements that form $3+Q/2$ classes.

(i) C_0, consisting of the identity element.

(ii) $Q/2-1$ two-element classes, C_n for $n=1,2,\ldots,Q/2-1$, each consisting of the rotations by $\pm 2n\pi/Q$ about the origin.

(iii) $C_{Q/2}$, consisting of rotation by π about the origin.

(iv) C_σ, consisting of the $Q/2$ reflections about lines of slope $\tan(2n\pi/Q)$.

(v) $C_{\sigma'}$, consisting of the $Q/2$ reflections about lines of slope $\tan[(2n+1)\pi/Q]$.

For these groups, the dimensionalities d_r of the $3+Q/2$ irreducible representations are completely determined by the well-known formula $\sum_r d_r^2=N$. The characters $\chi_r(C_l)$ of the operations in the class C_l in the representation r can be determined with the aid of the orthogonality relations $\sum_r \chi_r(C_k)\chi_r(C_l)=\delta_{kl}N/N_l$ and $\sum_l N_l\chi_r(C_l)\chi_s(C_l)=\delta_{rs}N$, where N_l is the number of elements in C_l. The decomposition of a product of a irreducible representations Γ^r and Γ^s into a direct of irreducible representations is given by the formula

$$\Gamma^r\otimes\Gamma^s=\sum_t a_{rst}\Gamma^t \ , \qquad a_{rst}=\frac{1}{N}\sum_l \chi_r(C_l)\chi_s(C_l)\chi_t(C_l) \ . \tag{32}$$

In the following subsections, the different orientational symmetries are treated. Owing to slight variations among the different symmetries, a completely unified treatment becomes too cumbersome. Nevertheless, the method of analysis and many of the results are quite similar and repetition of the details for all three cases is not necessary. The formalism developed in the discussion of the eightfold case extends in a straightforward way to the twelvefold and tenfold cases. All differences that arise are noted in the relevant subsection.

1. Eightfold symmetry

Table I shows the characters for the irrediculble representations of the point group C_{8v}. Each entry $\chi_r(C_l)$ is the character of the operations in the class C_l in the representation r. (The character is the trace of the d-dimensional matrices corresponding to the operations in a given class, where d is the dimension of r.) Recall that ∂ and $\mathbf{u}$ transform under Γ^2, the ordinary vector representation, and $\mathbf{w}$ transforms under $\Gamma^{\bar{2}}$.

The conventional strain tensor has both indices transforming like ordinary vectors. Equation (32) with $r=s=2$ implies that there exist $\mathbf{M}^{(u)}$'s of three different types, transforming under the representations Γ^1, Γ^{1a}, and Γ^{2a}. These are identified as compressions, rotations, and shears, respectively. Note that the continuous rotational symmetry of the free energy of the system implies that rotations do not contribute to the elastic energy.

In a similar manner, the irreducible phason strains can be identified. The phason strain tensor has one index transforming as an ordinary vector and the other as a "phasonlike" vector. Equation (32) with $r=2,s=\bar{2}$ implies that there exist $\mathbf{M}^{(w)}$'s of three different types, transforming under the representations Γ^{1b}, Γ^{1c}, and Γ^{2a}. For lack of a better idea, these are termed Γ^{1b}-strain, Γ^{1c}-strain, and Γ^{2a}-strain (respectively, of course). It is straightforward to show that the linear combinations of $\mathbf{e}_n\bar{\mathbf{e}}_m$ that transform irreducibly are

$$\begin{aligned}
\mathbf{M}^{(1b)}&=\frac{1}{\sqrt{2}}(e_0\bar{\mathbf{e}}_0+\mathbf{e}_2\bar{\mathbf{e}}_2)\\
&=-\frac{1}{\sqrt{2}}(\mathbf{e}_1\bar{\mathbf{e}}_1+\mathbf{e}_3\bar{\mathbf{e}}_3)\\
&=\frac{1}{\sqrt{2}}\begin{bmatrix}1&0\\0&1\end{bmatrix},\\
\mathbf{M}^{(1c)}&=\mathbf{e}_0\bar{\mathbf{e}}_1+\mathbf{e}_1\bar{\mathbf{e}}_0\\
&=-\mathbf{e}_1\bar{\mathbf{e}}_2-\mathbf{e}_2\bar{\mathbf{e}}_1\\
&=\mathbf{e}_2\bar{\mathbf{e}}_3+\mathbf{e}_3\bar{\mathbf{e}}_2\\
&=\mathbf{e}_3\bar{\mathbf{e}}_0+\mathbf{e}_0\bar{\mathbf{e}}_3\\
&=\frac{1}{\sqrt{2}}\begin{bmatrix}0&-1\\1&0\end{bmatrix},
\end{aligned} \tag{33}$$

and the pair

TABLE I. Characters of the group C_{8v}.

	E	$2C_1$	$2C_2$	$2C_3$	C_4	$4C_\sigma$	$4C_{\sigma'}$
Γ^1	1	1	1	1	1	1	1
Γ^{1a}	1	1	1	1	1	-1	-1
Γ^{1b}	1	-1	1	-1	1	1	-1
Γ^{1c}	1	-1	1	-1	1	-1	1
Γ^2	2	$\sqrt{2}$	0	$-\sqrt{2}$	-2	0	0
$\Gamma^{\bar{2}}$	2	$-\sqrt{2}$	0	$\sqrt{2}$	-2	0	0
Γ^{2a}	2	0	-2	0	2	0	0

$$\mathbf{M}_1^{(2a)}=\frac{1}{\sqrt{2}}(\mathbf{e}_0\bar{\mathbf{e}}_0-\mathbf{e}_2\bar{\mathbf{e}}_2)=\frac{1}{\sqrt{2}}\begin{bmatrix}1&0\\0&-1\end{bmatrix},$$
$$\mathbf{M}_2^{(2a)}=\frac{1}{\sqrt{2}}(\mathbf{e}_1\bar{\mathbf{e}}_1-\mathbf{e}_3\bar{\mathbf{e}}_3)=\frac{1}{\sqrt{2}}\begin{bmatrix}0&-1\\-1&0\end{bmatrix}. \quad (34)$$

(The explicit matrices in these formulas depend upon the choice of coordinates in the $\bar{\mathbf{e}}$ space. The ones listed correspond to the definitions in Fig. 3, where $\bar{\mathbf{e}}_0$ is taken as the positive x axis and $\bar{\mathbf{e}}_2$ as the y axis.)

The different types of uniform irreducible phason strains have distinguishable effects on both the tiling and its diffraction pattern. That is, it is possible to discover which types of irreducible strain are present by inspection of a tiling or its diffraction pattern. We consider first the diffraction pattern, then examine the real-space analogues of the results.

The diffraction pattern of an ideal (unstrained) eightfold PLI class tiling with tile edges of unit length consists of Bragg peaks at the wave vectors $\mathbf{q}=\sum_{n=0}^{3}2\pi k_n\mathbf{e}_n$, for all sets of integral k_n. (The intensities of the peaks depend on the details of the decorations of the tiles with scatterers). The notation $(k_0k_1k_2k_3)$ is used to represent the wave vector with indices k_n. Under a uniform phason strain $\mathbf{M}^{(w)}$, the peaks remain sharp, but are shifted in position, the peak at wave vector $\mathbf{q}$ being shifted to $\mathbf{q}+\mathbf{M}^{(w)}\cdot\bar{\mathbf{q}}$, where $\bar{\mathbf{q}}\equiv\sum_n k_n\bar{\mathbf{e}}_n$ for the same set of k_n's that define $\mathbf{q}$.[28] The analogous formula for conventional strains is $\mathbf{q}+\mathbf{M}^{(u)}\cdot\mathbf{q}$. Since $\bar{\mathbf{q}}$ is a wildly varying function of $\mathbf{q}$, uniform phason strains are easily distinguished from conventional strains. Given a set of peak positions and knowledge of the ideal positions it is straightforward to calculate $\mathbf{M}^{(u)}$ and $M^{(w)}$ and to decompose them into their irreducible components. The four elements of $\mathbf{M}^{(u)}$ and the four of $\mathbf{M}^{(w)}$ are determined by the vector shifts of any four integer linearly independent wave vectors.

it is well known that the two types of conventional strain, compressions and shears, are easily distinguished by inspection of the diffraction pattern; compression preserves the eightfold symmetry while shear breaks that symmetry. The different irreducible phason strains can also be distinguished quickly by inspection of the diffraction pattern. In anticipation of the discussion of the real-space tilings, it is useful to define the following quantities.

(i) $D_n\equiv\mathbf{e}_n\cdot\mathbf{M}^{(w)}\cdot\bar{\mathbf{e}}_n$. D_n is the magnitude of the $\mathbf{e}_n$ component of the shift of the peak at wave vector $\mathbf{e}_n$. (We will see below that D_n is related to the density of Ammann lines in the primary grid associated with $\mathbf{e}_n$.)

(ii) $J_n\equiv\mathbf{e}_n^{(r)}\cdot\mathbf{M}^{(w)}\cdot\bar{\mathbf{e}}_n$, where $\mathbf{e}_n^{(r)}$ is defined as the (counterclockwise) rotation of $\mathbf{e}_n$ through $\pi/2$. J_n is the magnitude of the shift of the peak at $\mathbf{e}_n$ in the direction perpendicular to $\mathbf{e}_n$. (J_n is also related to the density of jags in the primary grid associated with $\mathbf{e}_n$.)

(iii) D_{mn} and J_{mn} are defined as $\mathbf{f}_{nm}\cdot\mathbf{M}^{(w)}\cdot\bar{\mathbf{f}}_{nm}$ and $\mathbf{f}_{nm}^{(r)}\cdot\mathbf{M}^{(w)}\cdot\bar{\mathbf{f}}_{nm}$, respectively. They are related to the parallel and perpendicular shifts of the peak at $\mathbf{f}_{nm}$. (They are also related to the density of Ammann lines and jags in the secondary grid associated with $\mathbf{f}_{nm}$.)

Now for a 1D representation r, if $\chi_r(C_l)=1$, then an object transforming under this representation is invariant under the operations of C_l. Thus, $\mathbf{M}^{(1b)}$ is invariant under rotations by $\pi/2$ and under reflections about the $\mathbf{e}_n$ directions. This means that for Γ^{1b} strain, J_n must be zero for all n, as can easily be verified by direct computation. $J_n=0$ is a unique signature of Γ^{1b} strain. Similarly, $\mathbf{M}^{(1c)}$ is invariant under rotation by $\pi/2$ and under reflections about the $\mathbf{f}_{nm}$ directions, implying that for Γ^{1c} strain J_{mn} must be zero for all mn. Diffraction patterns exhibiting Γ^{1b} strain and Γ^{1c} strain are shown in Fig. 12. The size of a spot at $\mathbf{q}$ has been made inversely proportional to the magnitude of $\bar{\mathbf{q}}$. (Most quasicrystal models exhibit a nearly monotonic increase in intensity with decreasing $\|\bar{\mathbf{q}}\|$.)

The quantities J_n, D_n, J_{mn}, and D_{mn} have direct interpretations in terms of the real-space tiling. Consider first the strained primary Ammann quasilattice, which consists of the points $\mathbf{x}$ satisfying

$$\mathbf{x}\cdot\mathbf{e}_n=N+\alpha_n+\frac{1}{\omega}\left\lfloor\frac{N}{\omega}+\beta_n+\mathbf{w}\cdot\bar{\mathbf{e}}_n\right\rfloor$$
$$=N+\alpha_n+\frac{1}{\omega}\left\lfloor\frac{N}{\omega}+\beta_n+\mathbf{x}\cdot\mathbf{M}^{(w)}\cdot\bar{\mathbf{e}}_n\right\rfloor, \quad (35)$$

where α_n and β_n correspond to some member of the PLI class. For $D_n>(<)0$, as the $\mathbf{e}_n$ component of $\mathbf{x}$ is increased, $\mathbf{w}\cdot\bar{\mathbf{e}}_n$ increases (decreases) linearly. Thus with increasing N the argument of the greatest integer function increases faster (slower) than N/ω, which produces more (fewer) large spacings in the grid. A grid for which $D_n>0$ has a lower density of Ammann lines (more large spacings); one with $D_n<0$ has a higher density of Ammann lines. If $J_n\neq0$, then $\mathbf{w}\cdot\bar{\mathbf{e}}_n$ varies linearly as one moves along an Ammann line in the nth grid, creating jags in the line at each point where $N/\omega+\mathbf{w}\cdot\bar{\mathbf{e}}_n$ crosses an integer. The density of such jags is proportional to J_n. D_{mn} and J_{mn} affect the secondary Ammann quasilattice in exactly the same ways that D_n and J_n affect primary Ammann quasilattice.

Nonzero values of D and J are easily distinguished from the effects of conventional strains. Conventional strains affect the Ammann quasilattice through the terms $\alpha_n+\mathbf{e}_n\cdot\mathbf{u}(\mathbf{x})$ and produce changes in the slopes of the Ammann lines and in the values of the large and small spacings, but have no effect on the sequence of spacings. To fit the tiles to an Ammann quasilattice with such dis-

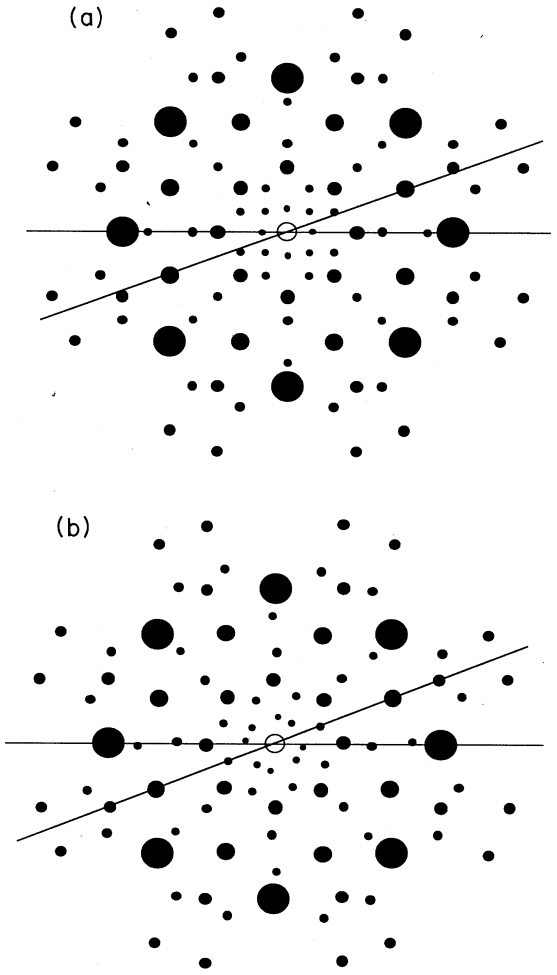

FIG. 12. Diffraction pattern for an eightfold quasicrystal with uniform phason strain. The lines show the (1000) and (1100) directions. In the unstrained pattern, peaks would align directly along these directions. The size of each dot is roughly proportional to the intensity of the peak. Note that the peaks of smaller intensity are shifted further from their ideal positions. (a) Γ^{1b} strain. The peaks in the (1000) directions remain in line, but those in the (1100) do not. (b) Γ^{1c} strain. The peaks in the (1100) directions remain in line, but those in the (1000) do not.

tortions, it is necessary to distort the shapes of the tiles; the effect of conventional strain on the tiling are exactly the same as familiar distortions of unit cells in strained crystals.

The fact that $J_n=0$ for all n in an eightfold tiling exhibiting pure Γ^{1b} strain implies that there are no violations of the edge-arrow matching rules in the tiling. An example of such a tiling is shown in Fig. 13(a). Note that this is an example of a periodic tiling with continuous primary Ammann lines, as is allowed by the reasoning in Sec. III B 5. The pattern does contain discontinuities in the secondary Ammann lines, though, as it must to be consistent with that same reasoning. It is also possible to construct a tiling with pure Γ^{1c} strain that has no secondary jags, as is shown in Fig. 13(b). On the other hand, Γ^{2a} strain necessarily contains both primary and secondary jags.

Of the sixteen quantities, J_n, J_{nm}, D_n, and D_{nm}, only four can be chosen independently, constraints on them arising from the relations among $\mathbf{e}_n$, $\mathbf{f}_{nm}$, $\bar{\mathbf{e}}_n$, and $\bar{\mathbf{f}}_{nm}$. Using $\mathbf{e}_1=(1/\sqrt{2})(\mathbf{e}_0+\mathbf{e}_2)$ and $\bar{\mathbf{e}}_1=(-1/\sqrt{2})(\bar{\mathbf{e}}_0+\bar{\mathbf{e}}_2)$, for example, it is straightforward to derive the identities

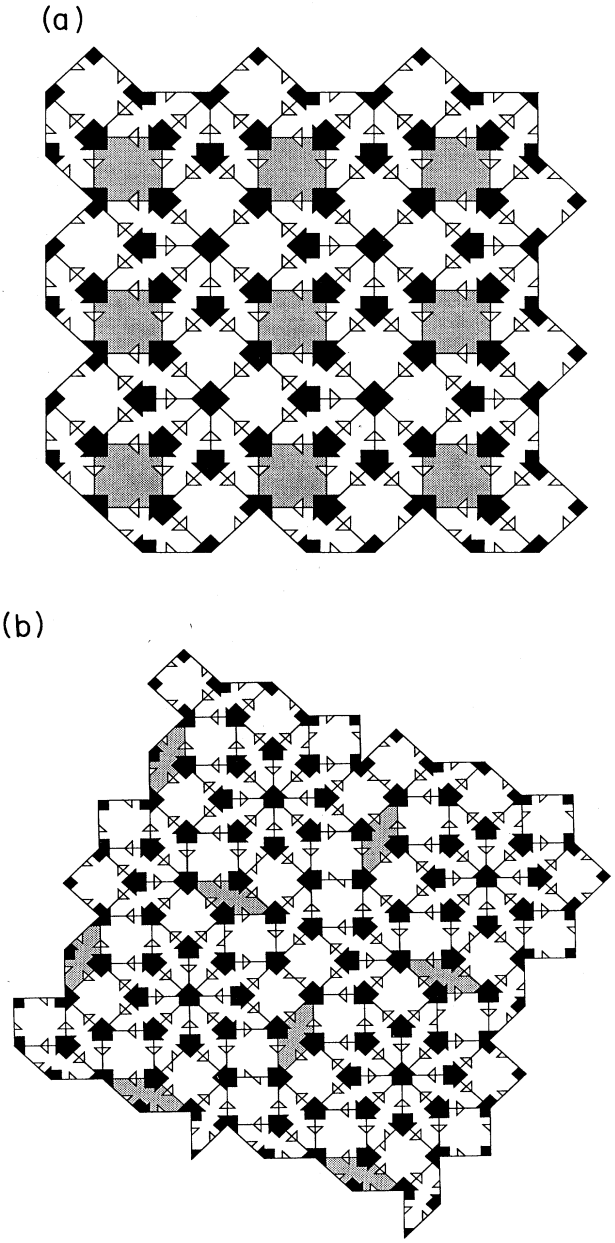

FIG. 13. Octagonal PLI class tilings with uniform phason strain. The strain magnitude has been chosen such that the pattern is periodic. The shaded tiles highlight the periodicity. (a) Γ^{1b} strain. There are no primary mismatches (no violations of the edge arrow matching rule). (b) Γ^{1c} strain. There are no secondary mismatches (no illegal vertex keys).

$$2D_1 = J_2 - J_0 - D_2 - D_0 ,$$
$$D_{01} = D_0 + D_1 + \frac{1}{\sqrt{2}}(J_0 + J_2) . \tag{36}$$

Cyclic permutation of the indices (0123) produces identities related to these by symmetry operations. Two important identities that can be derived from these are

$$\sum_n J_n = 0 \quad \text{and} \quad \sum_n D_n = 0 . \tag{37}$$

It is instructive to compute the number density of jags and the change in the densities of the different tile types as functions of J_n and D_n. To do so, we exploit the exact geometric relation between the Ammann quasilattice intersections and the tiles dual to them. The density of square tiles is given by the density of 90° intersections in the primary Ammann quasilattice, and the density of rhombi by the density of 45° intersections.

For the purposes of computing the densities of Ammann-line intersections, it is useful to define an "average grid" corresponding to each grid in the Ammann quasilattice. The average grid is a periodic grid composed of continuous lines with slope equal to the average slope of the Ammann lines with jags. The spacing between the lines is chosen to produce the same density of lines as is found in the Ammann quasilattice grid. A_n is defined as the spacing between lines in the average grid corresponding to the Ammann quasilattice grid with normal $\mathbf{e}_n$, $\mathbf{a}_n$ is the unit normal to the average grid, and ϕ_n is the angle between $\mathbf{e}_n$ and $\mathbf{a}_n$.

The density of intersections between lines of two average grids is easily calculated. Any two periodic grids with spacings A_n and A_m, considered by themselves, form a periodic lattice of parallelograms of area $A_n A_m / |\sin\theta|$, where θ is the angle between the normals to the grid lines. Thus the density of intersections between grids n and m in the Ammann quasilattice is equal to $|\sin(\theta_{mn} + \phi_m - \phi_n)| / (A_n A_m)$, where θ_{mn} is the angle between $\mathbf{e}_n$ and $\mathbf{e}_m$.

Recall that J_n and D_n are both of order ν, the magnitude of the phason strain tensor. We wish to compute the tile densities to leading order in ν. Consider first a grid for which J_n is zero but D_n is not. A_n can be derived from Eq. (35) by approximating $\mathbf{x}\cdot\mathbf{e}_n$ by $A_n N + \gamma$ and solving for A_n in the limit of large N:

$$A_n N + \gamma \approx S\left[N + \alpha_n + \frac{1}{\omega}\right]\left[\frac{N}{\omega} + (A_n N + \gamma) D_n + \beta_n\right] ,$$
$$\Rightarrow A_n + \frac{\gamma}{N} \approx S\left[1 + \frac{1}{\omega^2} + \frac{1}{\omega} A_n D_n\right] + O\left[\frac{1}{N}\right] , \tag{38}$$
$$\Rightarrow A_n = S\left[1 + \frac{1}{\omega^2}\right]\left[1 - \frac{1}{\omega} S D_n\right]^{-1} .$$

For $n = 0$ and nonzero J_0, the magnitude of the slope of the average grid lines, $|\tan\phi_0|$, is given by the width of a jag, S/ω, divided by the spacing between jags on the same line. A good approximation to the spacing between jags is the distance in the $\mathbf{e}_n^{(r)}$ direction over which $\mathbf{x}\cdot\nu\mathbf{M}^{(w)}\cdot\bar{\mathbf{e}}_n$ changes by unity, which is just $1/|J_n|$. Corrections to this arise if D_n is nonzero, since $\mathbf{w}$ varies slightly over the width of the jag, but such corrections will not enter the leading-order calculations. The sign of the slope is determined by the sign of J_n. For $J_n > (<) 0$, the Ammann line jags to the right (left) as it is traversed in the $\mathbf{e}_n^{(r)}$ direction. Thus $J_n > 0$ implies a positive value of $\tan\phi_n$, and we have simply

$$\tan\phi_n = S J_n / \omega . \tag{39}$$

A slight change in A_n, arising from the nonzero value of ϕ_n, will enter the lowest-order calculations. Some simple geometry reveals that A_n is given by $S(1+1/\omega^2)(1 - Dn/\omega)^{-1}\cos\phi_n$, which finally yields

$$A_n = S\left[1 + \frac{1}{\omega^2}\right]\left[1 - \frac{1}{\omega} S D_n\right]^{-1} (1 + S^2 J_n^2/\omega^2)^{-1/2} . \tag{40}$$

The number density of jags in a given grid is just the density along a single line, $|J_n|$, divided by the average spacing, A_n. The total density of jags in the Ammann quasilattice, ρ_J, is therefore given, to order ν, by

$$\rho_J = \sum_n \frac{|J_n|}{S(1+1/\omega^2)} . \tag{41}$$

The density of jags is linear in the strain magnitude.

The density of square tiles, ρ_s, is given by the sum of the densities of intersections of grids 0 and 2 and of grids 1 and 3:

$$\rho_s = \frac{\sin(\phi_2 - \phi_0 + \pi/2)}{A_0 A_2} + \frac{\sin(\phi_3 - \phi_1 + \pi/2)}{A_1 A_3}$$
$$= \frac{1 - (S/\omega)(D_0 + D_1 + D_2 + D_3) + (S^2/\omega^2)(J_0 J_2 + J_1 J_3 + D_0 D_2 + D_1 D_3)}{S^2(1+1/\omega^2)^2} \tag{42}$$

to second order in ν. Now, because of the identity $\sum_n D_n = 0$, the term linear in ν vanishes. It can be shown that the linear term in the density of rhombic tiles vanishes also. The gist of the argument is that if a term with denominator $A_n A_m$ occurs in the expression for the density of a given tile type [top line in Eq. (42)], then all terms $A_k A_l$ related to it by symmetry must appear. Hence the $(1 - D_n)$ terms generated from substitution of Eq. (40) into Eq. (42) come in symmetric sets, always producing a linear term proportional to $\sum_n D_n$. The conclusion is that even though the densities of lines in the individual grids include terms linear in D_n, the leading

term in the expansion of the tile densities about their ideal values is quadratic in the magnitude of the phason strain.

An exact formula for the changes in tile densities associated with phason strains has been obtained by Henley in the context of the projection construction.[29] The above calculation in terms of Ammann lines is in agreement with Henley's result.

2. *Twelvefold symmetry*

Table II shows the characters for the irreducible representations of the point group C_{12v}. The similarity between this case and that of C_{8v} is quite extensive: ∂ and $\mathbf{u}$ transform under Γ^2, and $\mathbf{w}$ transforms under $\Gamma^{\bar{2}}$, there exist $\mathbf{M}^{(u)}$'s transforming under the representations Γ^1, Γ^{1a}, and Γ^{2a} corresponding to compressions, rotations, and shears, respectively, and there exist $\mathbf{M}^{(w)}$'s of three different types, transforming under the representations Γ^{1b}, Γ^{1c}, and Γ^{2b}.

The linear combinations of $\mathbf{e}_n\bar{\mathbf{e}}_m$ that transform irreducibly are

$$\begin{aligned}
\mathbf{M}^{(1b)} &= \frac{1}{\sqrt{2}}(\mathbf{e}_0\bar{\mathbf{e}}_0-\mathbf{e}_3\bar{\mathbf{e}}_3)\\
&= -\frac{1}{\sqrt{2}}(-\mathbf{e}_1\bar{\mathbf{e}}_1+\mathbf{e}_4\bar{\mathbf{e}}_4)\\
&= -\frac{1}{\sqrt{2}}(\mathbf{e}_2\bar{\mathbf{e}}_2-\mathbf{e}_5\bar{\mathbf{e}}_5)\\
&= \frac{1}{\sqrt{2}}\begin{bmatrix}1 & 0\\ 0 & -1\end{bmatrix},\\
\mathbf{M}^{(1c)} &= \frac{1}{\sqrt{2}}(\mathbf{e}_0\bar{\mathbf{e}}_3+\mathbf{e}_3\bar{\mathbf{e}}_0)\\
&= \frac{1}{\sqrt{2}}(\mathbf{e}_1\bar{\mathbf{e}}_4+\mathbf{e}_4\bar{\mathbf{e}}_1)\\
&= \frac{1}{\sqrt{2}}(\mathbf{e}_2\bar{\mathbf{e}}_5+\mathbf{e}_5\bar{\mathbf{e}}_2)\\
&= \frac{1}{\sqrt{2}}\begin{bmatrix}0 & -1\\ -1 & 0\end{bmatrix},
\end{aligned} \tag{43}$$

and the pair

$$\begin{aligned}
\mathbf{M}_1^{(2b)} &= \frac{1}{\sqrt{2}}(\mathbf{e}_0\bar{\mathbf{e}}_0+\mathbf{e}_3\bar{\mathbf{e}}_3)\\
&= \sqrt{2}(-\mathbf{e}_1\bar{\mathbf{e}}_1-\mathbf{e}_2\bar{\mathbf{e}}_2)\\
&= \sqrt{2}(-\mathbf{e}_4\bar{\mathbf{e}}_4-\mathbf{e}_5\bar{\mathbf{e}}_5)\\
&= \frac{1}{\sqrt{2}}\begin{bmatrix}1 & 0\\ 0 & 1\end{bmatrix},\\
\mathbf{M}_2^{(2b)} &= \frac{1}{\sqrt{2}}(\mathbf{e}_0\bar{\mathbf{e}}_3-\mathbf{e}_3\bar{\mathbf{e}}_0)\\
&= \sqrt{2}(-\mathbf{e}_1\bar{\mathbf{e}}_4+\mathbf{e}_2\bar{\mathbf{e}}_5)\\
&= \sqrt{2}(\mathbf{e}_4\bar{\mathbf{e}}_1-\mathbf{e}_5\bar{\mathbf{e}}_2)\\
&= \frac{1}{\sqrt{2}}\begin{bmatrix}0 & 1\\ -1 & 0\end{bmatrix}.
\end{aligned} \tag{44}$$

The identity $\mathbf{e}_0\bar{\mathbf{e}}_3-\mathbf{e}_3\bar{\mathbf{e}}_0=\sqrt{3}/2(\mathbf{e}_4\bar{\mathbf{e}}_4+\mathbf{e}_2\bar{\mathbf{e}}_2)$ and others related to it by symmetry are useful for checking that $\mathbf{M}_1^{(2b)}$ and $\mathbf{M}_2^{(2b)}$ transform into linear combinations of each other. The identity is itself easily verified by writing out the matrices explicitly.

As in the case of eightfold symmetry, Γ^{1b} strain yields $J_n=0$ for all n and Γ^{1c} strain yields $J_{nm}=0$ for all nm. Examples of typical diffraction patterns with the different irredicuble phason strains are shown in Fig. 14 and tilings exhibiting Γ^{1b} and Γ^{1c} strain are shown in Fig. 15. Once again there are no primary jags for $\mathbf{M}^{(1b)}$ and no secondary jags for $\mathbf{M}^{(1c)}$.

The extension of the jag density and tile density analysis to the twelvefold case is straightforward. The principal conclusions, that the jag density goes like the strain magnitude while the tile densities go like the square of the strain magnitude, are unaltered. Note, however, that because $\sigma'<0$ for the twelvefold case, $D_n>0$ implies more short intervals and $J_n>0$ implies jags to the left. The analogues of the identities of Eq. (36) are

$$\begin{aligned}
4D_1 &= D_3-3D_0-\sqrt{3}(J_3+J_0)\ ;\\
2D_{01} &= 2D_0+2D_1-J_3-J_0\ .
\end{aligned} \tag{45}$$

We still have $\sum_n J_n=\sum_n D_n=0$.

TABLE II. Characters of the group C_{12v}.

	E	$2C_1$	$2C_2$	$2C_3$	$2C_4$	$2C_5$	C_6	$6C_\sigma$	$6C_{\sigma'}$
Γ^1	1	1	1	1	1	1	1	1	1
Γ^{1a}	1	1	1	1	1	1	1	−1	−1
Γ^{1b}	1	−1	1	−1	1	−1	1	1	−1
Γ^{1c}	1	−1	1	−1	1	−1	1	−1	1
Γ^2	2	$\sqrt{3}$	1	0	−1	$-\sqrt{3}$	−2	0	0
$\Gamma^{\bar{2}}$	2	$-\sqrt{3}$	1	0	−1	$\sqrt{3}$	−2	0	0
Γ^{2a}	2	1	−1	−2	−1	1	2	0	0
Γ^{2b}	2	−1	−1	2	−1	−1	2	0	0
Γ^{2c}	2	0	−2	0	2	0	−2	0	0

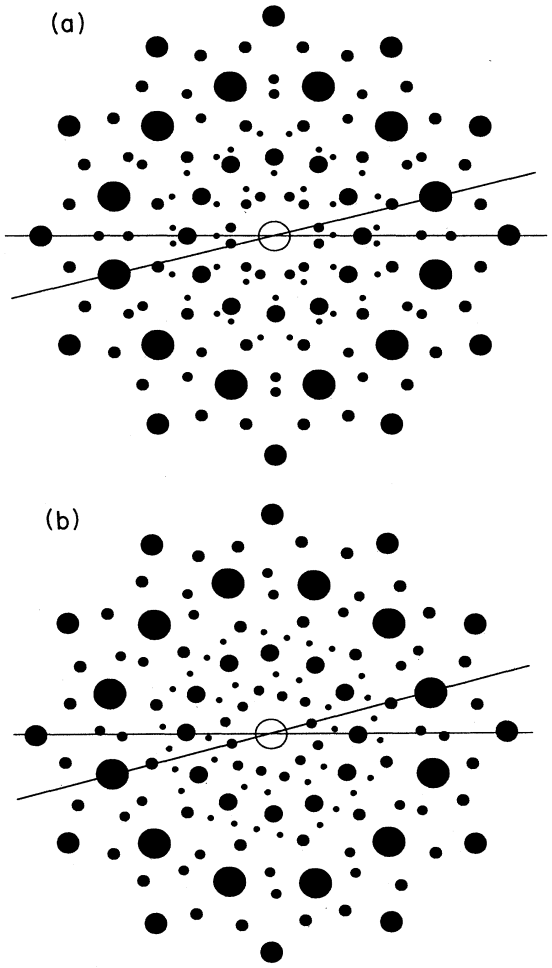

FIG. 14. Diffraction pattern for the twelvefold quasicrystal with uniform phason strain. The lines show the (100000) and (110000) directions. In the unstrained pattern, peaks would align directly along these directions. The size of each dot is roughly proportional to the intensity of the peak. Note that the peaks of smaller intensity are shifted further from their ideal positions. (a) Γ^{1b} strain. The peaks in the (100000) directions remain in line, but those in the (110000) do not. (b) Γ^{1c} strain. The peaks in the (110000) directions remain in line, but those in the (100000) do not.

TABLE III. Characters of the group C_{10v}.

	E	$2C_1$	$2C_2$	$2C_3$	$2C_4$	C_5	$5C_\sigma$	$5C_{\sigma'}$
Γ^1	1	1	1	1	1	1	1	1
Γ^{1a}	1	1	1	1	1	1	−1	−1
Γ^{1b}	1	−1	1	−1	1	−1	1	−1
Γ^{1c}	1	−1	1	−1	1	−1	−1	1
Γ^2	2	τ	$\frac{1}{\tau}$	$-\frac{1}{\tau}$	$-\tau$	−2	0	0
$\Gamma^{\bar{2}}$	2	$-\frac{1}{\tau}$	$-\tau$	τ	$\frac{1}{\tau}$	−2	0	0
Γ^{2a}	2	$\frac{1}{\tau}$	$-\tau$	$-\tau$	$\frac{1}{\tau}$	2	0	0
Γ^{2b}	2	$-\tau$	$\frac{1}{\tau}$	$\frac{1}{\tau}$	$-\tau$	2	0	0

3. *Tenfold symmetry*

Table III shows the characters for the irredicuble representations of the point group C_{10v}. There are significant differences between this case and the others, as might have been anticipated from the geometric argument of Sec. III B. The fact that a secondary Ammann quasilattice is not necessary for enforcing the matching rules suggests that all uniform phason strains produce primary jags, and this is indeed the case. Though the analysis of conventional strains in the tenfold case mirrors quite closely that of the eightfold and twelvefold cases, it is found that there exists only two types of irredicuble phason strain, transforming under Γ^2 and $\Gamma^{\bar{2}}$.

The easiest way to distinguish between Γ^2 strain and $\Gamma^{\bar{2}}$ strain is to examine the signs of D_n. Figure 16 shows the patterns produced by Γ^2 and $\Gamma^{\bar{2}}$ strain. The sign of D_n is marked at both $\mathbf{e}_n$ and $-\mathbf{e}_n$. Γ^2 strain produces a dipolelike pattern that has the appropriate symmetry for coupling to shears, while $\Gamma^{\bar{2}}$ strain does not. Of course, the phonon and phason strain matrices can be determined completely from measurement of J_n and D_n for four values of n and we again have $\sum_n J_n = \sum_n D_n = 0$.

V. ENERGETICS OF PHASON STRAIN

The question of how the free energy of a quasicrystal depends on the phason strains present involves several subtleties that are not fully understood. The most immediate problem is that the conditions under which the usual harmonic approximation to the free-energy density is applicable are not known. This issue will not be resolved here. The canonical elasticity theory, based on the harmonic form of the free energy, is presented because it may well apply to physical systems and, in any case, is a useful reference point for the discussion of other forms of the free energy. Following the treatment of the harmonic free energy, the question of whether it is applicable to quasicrystals that are well described by ordered tilings is briefly discussed.

A. Canonical elasticity theory

Standard treatment of elasticity theory begins with the assumption that the free-energy density $F_{\rm el}$ to lowest order in the strain magnitude is a quadratic function of the strain. The theory then applies to strains of small enough amplitude that higher-order terms can be neglected. Under this assumption, the most general form of $F_{\rm el}$ for a 2D quasicrystal with eightfold, tenfold, or twelvefold symmetry is

$$F_{\rm el} = K^{(u)}_{ijkl}(\partial_i \mathbf{u}_j)(\partial_k \mathbf{u}_l) + K^{(w)}_{ijkl}(\partial_i \mathbf{w}_j)(\partial_k \mathbf{w}_l) + K^{(uw)}_{ijkl}(\partial_i \mathbf{u}_j)(\partial_k \mathbf{w}_l) , \quad (46)$$

where the elastic tensor $K^{(x)}_{ijkl}$ is a constant with elements determined by the details of the system. For a phason strain $\nu \mathbf{M}^{(w)}_{ij}$, where ν is the magnitude of the strain and $\mathbf{M}^{(w)}$ is normalized, the pure phason strain contribution takes the form $K^{(w)}_{ijkl}\nu^2 \mathbf{M}^{(w)}_{ij}\mathbf{M}^{(w)}_{kl}$.

The requirement that $F_{\rm el}$ behave as a scalar under the orientational symmetry group of the quasicrystal imposes

severe constraints on the elements of the elastic tensors. One independent element (called an elastic constant) exists for every identity representation occurring in the decomposition of $(\partial_i \mathbf{u}_j)(\partial_k \mathbf{u}_l)$, $(\partial_i \mathbf{w}_j)(\partial_k \mathbf{w}_l)$, and $(\partial_i \mathbf{u}_j)(\partial_k \mathbf{w}_l)$ into irredicuble representations.

Consider first the eightfold case. For conventional strains, we have $\partial\mathbf{u}$ transforming under $\Gamma^1 \oplus \Gamma^{2a}$, implying that $\partial\mathbf{u}\partial\mathbf{u}$ transforms under $(\Gamma^1 \oplus \Gamma^{2a}) \otimes (\Gamma^1 \oplus \Gamma^{2a})$. (Recall that the Γ^{1a} terms are just rotations and cannot contribute to $F_{\rm el}$.) Two identity representations arise, one from the $\Gamma^1 \otimes \Gamma^1$ term and one from the $\Gamma^{2a} \otimes \Gamma^{2a}$ term. The elastic constants associated with these contributions to $F_{\rm el}$ are the familiar bulk and shear moduli, respectively. For phason strains, similar reasoning yields three elastic constants that determine the energies of the three types of phason strain. Finally, the Γ^{2a} pieces of $\partial\mathbf{u}$ and $\partial\mathbf{w}$ combine to produce a scalar, so there is one elastic constant associated with the coupling of shears and Γ^{2a} strain, which will be referred to as the phonon-phason coupling constant. Thus there are a total of six elastic constants in a generic eightfold quasicrystal. In the tenfold case, the situation is similar to that of the eightfold case, but there are five elastic constants: the bulk and shear moduli, two phason elastic constants, and one phonon-phason coupling constant.

The twelvefold case has one significant and unexpected feature. There are, as for the eightfold case, bulk and shear moduli and three phason elastic constants. In the twelvefold case, however, the 2D representations corresponding to shears (Γ^{2a}) and to phason strains (Γ^{2b}) are

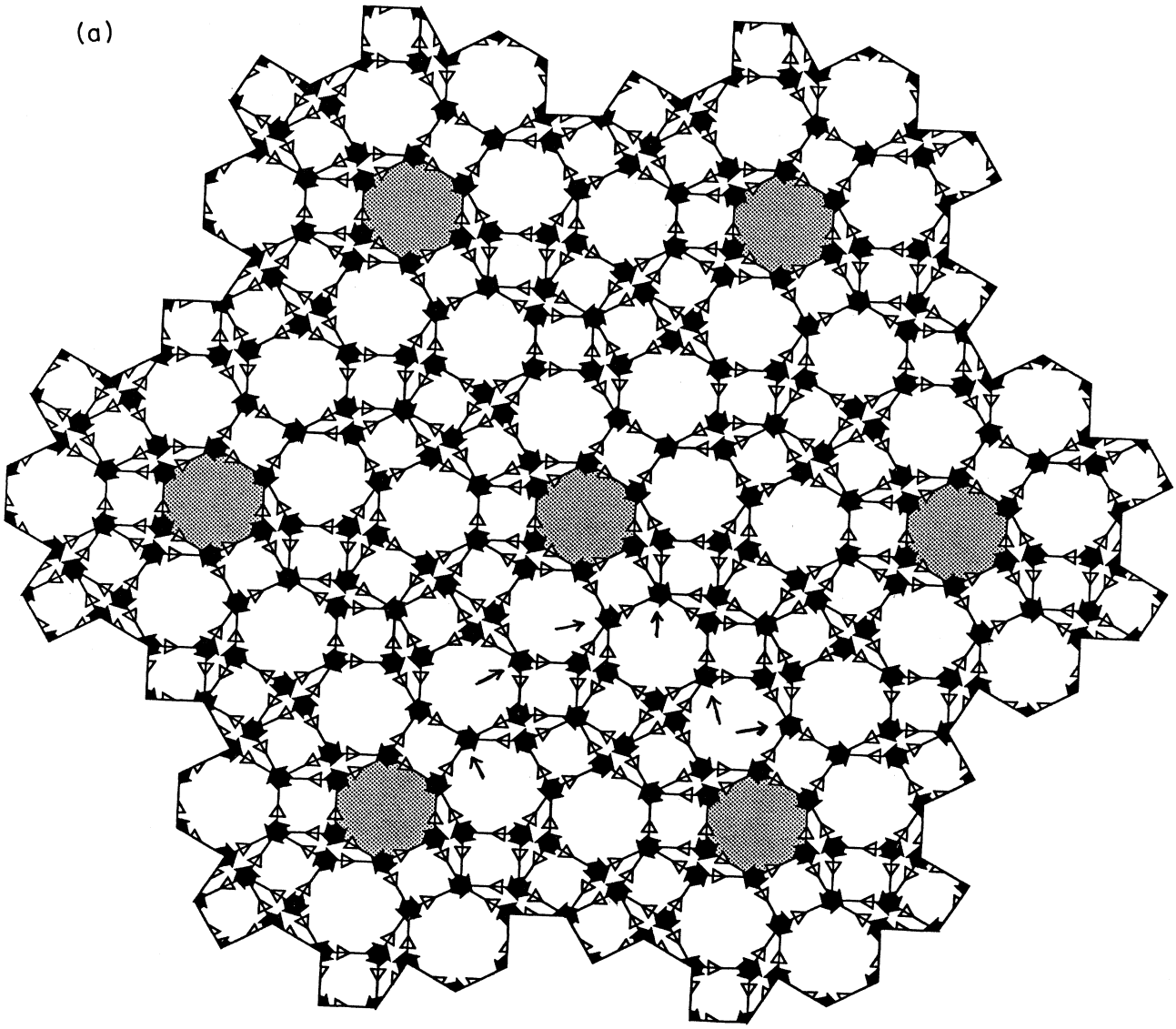

FIG. 15. Dodecagonal PLI class tilings with uniform phason strain. The strain magnitude has been chosen such that the pattern is periodic. The shaded tiles highlight the periodicity. (a) Γ^{1b} strain. There are no primary mismatches (no violations of the edge arrow matching rule). The small arrows point to the secondary mismatches (illegal vertex keys) within a single unit cell of the periodic structure. (b) Γ^{1c} strain. There are no secondary mismatches (no illegal vertex keys).

not the same and so they cannot be coupled to form a scalar term. *There is therefore no phonon-phason coupling in the harmonic approximation to the free energy of a twelve-fold quasicrystal.*

Further analysis of the quadratic invariants corresponding to the different phason elastic constants is revealing. For all three symmetries under consideration, there is a linear combination of the invariants that has the form of a total divergence. (See Ref. 30 for a discussion of the decagonal case.) Following the convention of Refs. 21 and 30, let $\partial_i \mathbf{w}_j$ be denoted by w_{ij}, or

$$\nu\mathbf{M}^{(w)}=\begin{bmatrix} w_{xx} & w_{xy} \\ w_{yx} & w_{yy} \end{bmatrix} . \tag{47}$$

The invariant linear combinations of w_{ij}'s corresponding to the different types of phason strain are readily constructed from Eqs. (33), (34), (43), and (44). Any phason strain $\nu\mathbf{M}^{(w)}$ can be written as

$$\nu\mathbf{M}^{(w)}=c_{1b}\mathbf{M}^{1b}+c_{1c}\mathbf{M}^{1c}+c_{2x,1}\mathbf{M}_1^{2x}+c_{2x,2}\mathbf{M}_2^{2x} , \tag{48}$$

where $x=a$ for the eightfold case and b for the twelvefold

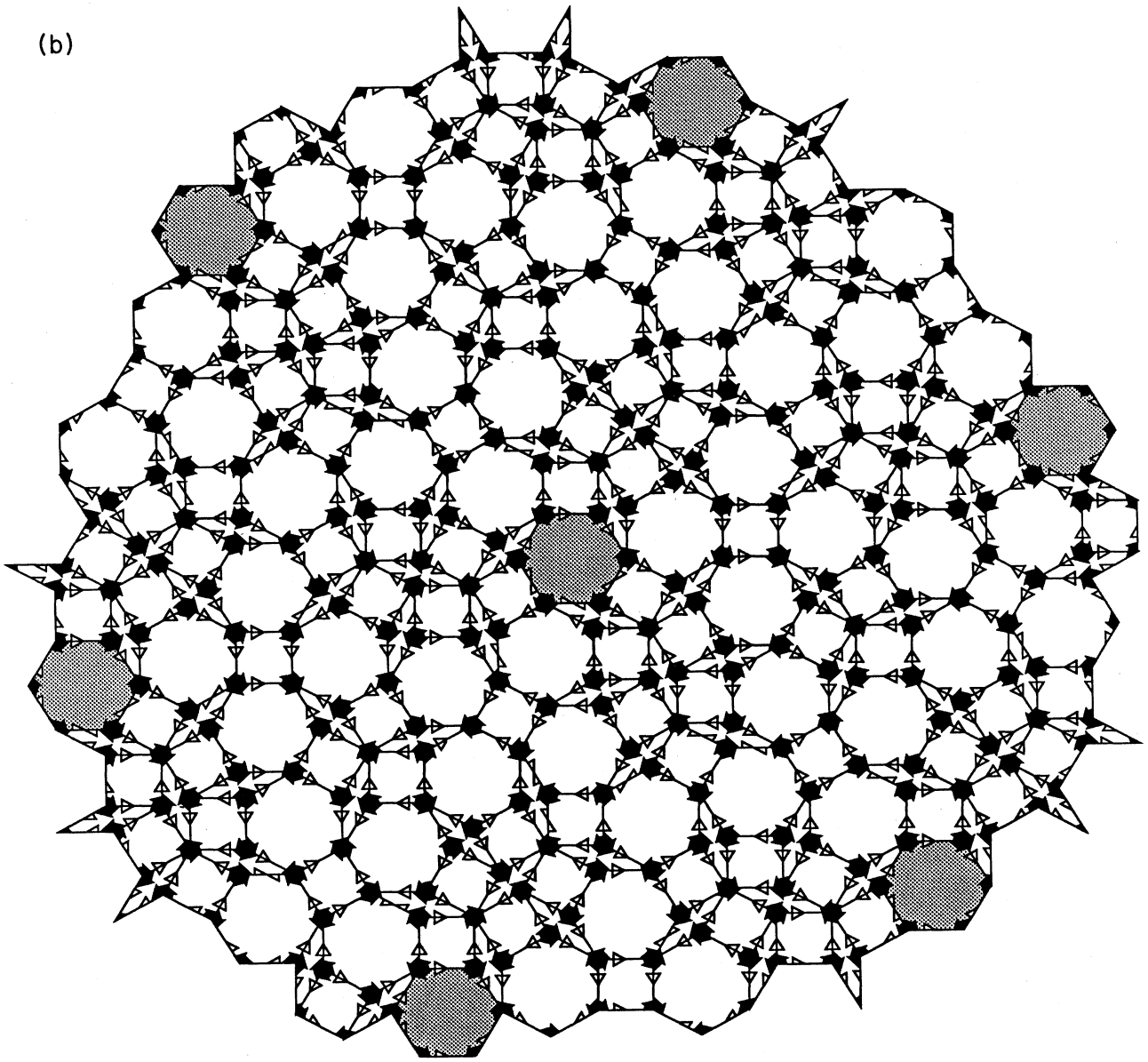

FIG. 15. (*Continued*).

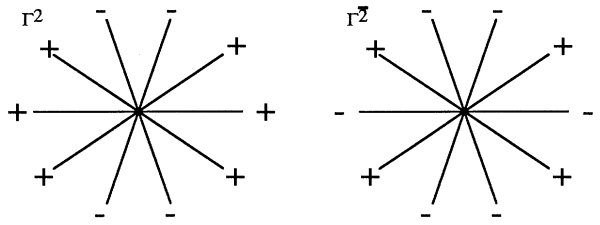

FIG. 16. Signs of D_n for generic uniform phason strains in a decagonal quasicrystal. A positive (negative) value of D_n indicates an increased (decreased) density of Ammann lines with normal $\mathbf{e}_n$. (a) Γ^2 strain. The pattern has the symmetry of a dipole and allows coupling to shears in the harmonic approximation to the free energy. (b) $\Gamma^{\bar{2}}$ strain. The symmetry of the pattern does not allow coupling to shears in the harmonic approximation.

case. The three invariant quantities corresponding to the identity representations in the reduction of $\nu^2 \mathbf{M}_{ij}^{(w)} \mathbf{M}_{kl}^{(w)}$ are $I_1 = c_{1b}^2$, $I_{1c} = c_{1c}^2$, and $I_{2x} = c_{2x,1}^2 + c_{2x,2}^2$. For the eightfold case, we have

$$\begin{aligned} I_{1b} &= w_{xx}w_{xx} + w_{yy}w_{yy} + 2w_{xx}w_{yy} \ , \\ I_{1c} &= w_{xy}w_{xy} + w_{yx}w_{yx} - 2w_{xy}w_{yx} \ , \\ I_{2a} &= w_{xx}w_{xx} + w_{yy}w_{yy} - 2w_{xx}w_{yy} \\ &\quad + w_{xy}w_{xy} + w_{yx}w_{yx} + 2w_{xy}w_{yx} \ , \end{aligned} \tag{49}$$

and for the twelvefold case, we have

$$\begin{aligned} I_{1b} &= w_{xx}w_{xx} + w_{yy}w_{yy} - 2w_{xx}w_{yy} \ , \\ I_{1c} &= w_{xy}w_{xy} + w_{yx}w_{yx} + 2w_{xy}w_{yx} \ , \\ I_{2b} &= w_{xx}w_{xx} + w_{yy}w_{yy} + 2w_{xx}w_{yy} \\ &\quad + w_{xy}w_{xy} + w_{yx}w_{yx} - 2w_{xy}w_{yx} \ . \end{aligned} \tag{50}$$

In terms of these invariants, the expression for $F_{\rm el}$ is

$$F_{\rm el} = K_{1b}I_{1b} + K_{1c}I_{1c} + K_{2x}I_{2x} \ . \tag{51}$$

Since each of the I's is a perfect square and therefore positive, the condition that constant $\mathbf{w}$ be a unique minimum of the free energy simply implies that each elastic constant K_x is positive definite.

Now the definition of the elastic constants is not unique; any three independent linear combinations of the invariants can be used to express $F_{\rm el}$. The choices of Eqs. (49) and (50) are convenient in that they are associated with irreducible strains, but they tend to obscure an important fact. Let us express F_{el} in terms of the following three linear combinations of I_{1b}, I_{1c}, and I_{2x}:

$$\begin{aligned} I_\alpha &\equiv (I_{1b} + I_{1c} + I_{2x})/2 \\ &= w_{xx}^2 + w_{yy}^2 + w_{xy}^2 + w_{yx}^2 \ , \\ I_\beta &\equiv I_{1b} - I_{1c} \\ &= (w_{xx} \pm w_{yy})^2 - (w_{xy} \mp w_{yx})^2 \ , \\ I_\gamma &\equiv (I_{1b} + I_{1c} - I_{2x})/2 \\ &= \pm 2(w_{xx}w_{yy} - w_{xy}w_{yx}) \ , \end{aligned} \tag{52}$$

where the upper sign always refers to the eightfold case and the lower to the twelvefold case. Note that I_α is just equal to ν^2. Inverting Eq. (52) and substituting into Eq. (51) yields

$$F_{\rm el} = K_\alpha I_\alpha + K_\beta I_\beta + K_\gamma I_\gamma \ ,$$

$$\text{with} \begin{cases} K_\alpha = (K_{1b} + K_{1c} + K_{2x})/2, & \text{(53a)} \\ K_\beta = (K_{1b} - K_{1c})/2, & \text{(53b)} \\ K_\gamma = K_{1b} + K_{1c} - K_{2x} \ . & \text{(53c)} \end{cases}$$

Note that these alternate elastic constants need not be positive, although there are constraints on them that follow from the positivity of the original ones.

The reason for reexpressing $F_{\rm el}$ is that in both the eightfold and twelvefold cases, I_γ is a total divergence and, in the absence of dislocations, can be integrated by parts and expressed as a boundary term. (In the tenfold case, there is also a term that can be integrated by parts.[30]) For uniform phason strains, the boundary term has no special significance. The contribution to the free energy from the boundary integration is an essential portion of the total. The boundary term is *not* a topological term; i.e., the quantity whose divergence is I_γ cannot be expressed as the gradient of a scalar, so integration of it along a closed loop does not necessarily yield zero in the absence of dislocations. For strains having wavelengths smaller than the sample size, however, the contribution of the boundary term goes like the ratio of the perimeter of the sample to its area and hence is negligible for large samples.

B. The discrete tiling model

Consider a quasicrystal with a zero-temperature ground state that is well described by a decoration of a PLI class tiling with atoms and assume for the moment that it is held at zero temperature. Since no two tiles, and therefore no two atoms, have identical infinite environments, the precise location of the atoms on each tile will vary slightly with this description must be only an approximation to the true ground state. We will assume that it is a good approximation, as seems reasonable in light of the relatively few local environments of the different tiles and the constraints of local atomic forces.

Now the energy associated with pure conventional strains derives from the displacement of atoms within harmonic wells that define their equilibrium configuration and therefore the energy is harmonic in the gradients of $\mathbf{u}$. The energy associated with pure phason strain, however, stems from two distinct sources: jags in the Ammann lines (or isolated violations of the matching rules) and deviations from the ideal sequence of spacings of the Ammann lines (or changes in the spatial distributions of tiles of different types and orientations). Even with no phonon-phason coupling, the question of how to

assign energies to the two effects is rather subtle and has not been resolved fully.

In the most trivial model of a stable quasicrystal at zero temperature, each violation of an edge-arrow matching rule costs a discrete energy, $\varepsilon_1 > 0$, and each violation of a vertex key matching rule costs a discrete energy, $\varepsilon_2 > 0$. The total energy of the system is just $E_T = L^2(\rho_1\varepsilon_1 + \rho_2\varepsilon_2)$, where ρ_1 and ρ_2 are the densities of jags in the primary and secondary Ammann quasilattices, respectively, and L^2 is the area of the sample. Using the results of Sec. IV B and the decomposition of $\mathbf{M}^{(w)}$ in Eq. (48), we find for the eightfold case (at zero temperature)

$$
\begin{aligned}
F_{\rm el} &\propto \varepsilon_1 \sum_n |\mathbf{e}_n^{(r)} \cdot \nu \mathbf{M}^{(w)} \cdot \bar{\mathbf{e}}_n| + \varepsilon_2 \sum_{nm} |\mathbf{f}_{nm}^{(r)} \cdot \nu \cdot \mathbf{M}^{(w)} \bar{\mathbf{f}}_{nm}| + O(\nu^2) \\
&= \varepsilon_1 (|c_{1c} + c_{2a,1}| + |c_{1c} - c_{2a,1}| + |c_{1c} + c_{2a,2}| + |c_{1c} - c_{2a,1}|) \\
&\quad + \varepsilon_2 \sqrt{2} \left(\left| c_{1b} + \frac{1}{\sqrt{2}}(c_{2a,1} + c_{2a,2}) \right| + \left| c_{1b} - \frac{1}{\sqrt{2}}(c_{2a,1} + c_{2a,1}) \right| \right. \\
&\quad \left. + \left| c_{1b} + \frac{1}{\sqrt{2}}(c_{2a,1} - c_{2a,2}) \right| + \left| c_{1b} - \frac{1}{\sqrt{2}}(c_{2a,1} - c_{2a,1}) \right| \right) . \qquad (54)
\end{aligned}
$$

The analogous result for the twelvefold case is

$$
\begin{aligned}
F_{\rm el} &= \varepsilon_1 [|c_{1c} + c_{2b,2}| + |c_{1c} - c_{2b,2}| + |c_{1c} + \tfrac{1}{2}(\sqrt{3} c_{2b,1} + c_{2b,2})| + |c_{1c} - \tfrac{1}{2}(\sqrt{3} c_{2b,1} + c_{2b,1})| \\
&\quad + |c_{1c} + \tfrac{1}{2}(\sqrt{3} c_{2b,1} - c_{2b,2})| + |c_{1c} - \tfrac{1}{2}(\sqrt{3} c_{2b,1} - c_{2b,1})|] \\
&\quad + \varepsilon_2 [|c_{1b} + c_{2b,2}| + |c_{1c} - c_{2b,2}| + |c_{1b} + \tfrac{1}{2}(\sqrt{3} c_{2b,1} + c_{2b,2})| + |c_{1b} - \tfrac{1}{2}(\sqrt{3} c_{2b,1} + c_{2b,1})| \\
&\quad + |c_{1b} + \tfrac{1}{2}(\sqrt{3} c_{2b,1} - c_{2b,2})| + |c_{1b} - \tfrac{1}{2}(\sqrt{3} c_{2b,1} - c_{2b,1})|] . \qquad (55)
\end{aligned}
$$

Note that the energy of a given strain is proportional to the strain magnitude, ν, rather than to ν^2, so that the results of the preceding section clearly do not apply. It is still true, of course, that strains related by a symmetry group operation have equal energies, but it is no longer true that the energy of a linear combination of two strains is equal to the same linear combination of their individual energies. For example, it is not true that all Γ^{2x} strains have the same energy.

An additional contribution to $F_{\rm el}$ arises if there is a difference between the binding energies of the atomic clusters that decorate tiles of different types; i.e., if it is energetically favorable to increase the density of one type of tile at the expense of another. In Sec. IV B, it was shown that the leading term for this effect is proportional to ν^2, suggesting a contribution to $F_{\rm el}$ of the canonical form.

The simple model discussed so far corresponds to a limit in which the atomic decoration of a tile is independent of the neighborhood of the tile, regardless of whether it is adjacent to a mismatch. Even within this limit, a more realistic model might include different energies for mismatches occurring between different types of tiles or at different types of vertices. The general form of the phason elastic contributions to $F_{\rm el}$ would not be altered; however, the energy would still be linear in the strain magnitude.

We must now consider two types of deviation from the limit. First, the effects of the relaxation of the atomic positions in the vicinity of a mismatch must be taken into account. If there is significant relaxation of atoms within a distance d from the mismatch, then mismatches separated by less than d will interact. If d is larger than the dimensions of the sample, a crossover to the canonical form of the elastic energy could conceivably result. At present, there is no conclusive understanding of the factors that influence d. Geometric arguments indicate that the motion of atoms corresponding to *uniform shifts* in $\mathbf{w}$ must be discontinuous,[13] and this *may* imply that the interactions between mismatches must fall off exponentially with their separation, but rigorous conclusions have yet to be drawn concerning configurations in which $\mathbf{w}$ is spatially varying.

Second, the effects of nonzero temperature on the free energy must be evaluated. Recall that each mismatch lies on a worm segment. Now in the absence of interactions between mismatches, the energy of the mismatch is independent of its precise position along the segment. Thus for nonzero temperature there is a nonzero entropic contribution to the free energy of a phason strain. It has been noted that the contribution to the entropy from a single mismatch goes like $\ln L_w$, where L_w is the length of the worm segment on which the mismatch resides, and that there always exist worm segments long enough so that $\ln L_w$ dominates the energy cost of the mismatch.[31] This suggests that a system containing noninteracting, discrete mismatches is unstable to fluctuations in the phason field at very large wavelengths. Note, however, that in a solid composed of periodically stacked quasicrystalline layers, the energy of a mismatch goes like the thickness of the sample in the periodic direction, since the Ammann lines are now planes perpendicular to the quasicrystal layers. For thick samples, one would therefore expect the entropic contribution to the free energy to

be dominated by the energy of the mismatch.

Clarification of these issues is critical to the understanding of the dynamics of the phason field. Standard hydrodynamic treatments based on the canonical form of F_{el} suggest that relaxation of long-wavelength variations in $\mathbf{w}$ is extremely slow, perhaps unobservable on experimental time scales.[32] If this is correct, production of a well-ordered quasicrystal would require a growth mechanism that avoids the introduction of phason strains during solidification.

VI. CONCLUSIONS

It is worth emphasizing again that the PLI class tilings discussed in this paper, though they play a special role in the analysis of the symmetries of interest here, are not necessarily priveleged candidates for modeling physical structures. It is possible that a different LI class would be required for the description of a given physical material. Nevertheless, the simplicity of the PLI class structures makes them easy to work with and allows the fundamental problems to come to the surface, unobscured by inessential complexities. Furthermore, it should be noted that many apparently unrelated structures can be viewed as decorations of the PLI class tilings, including many that are derived from projection of a hypercubic lattice using acceptance domains different from the unit hypercube. Figure 17 illustrates an example: the tiling underlying the structure proposed in Ref. 33 as a model for the dodecagonal phase of Ni-Cr is shown to be realizable as a simple decoration of the twelvefold PLI class tiling. Once such a decoration is obtained, the results detailed in this paper can be brought to bear on the analysis of the structure. For example, the configurations corresponding to phason strains can be identified and distinguished from other rearrangements of tiles. Also, one can ask whether the atomic decorations of the tiles break the mirror symmetries in a manner that would allow them to act as matching rules. (The specific model of Ref. 33 does not embody the complete set of matching rules, but minor refinements may be sufficient to incorporate them.)

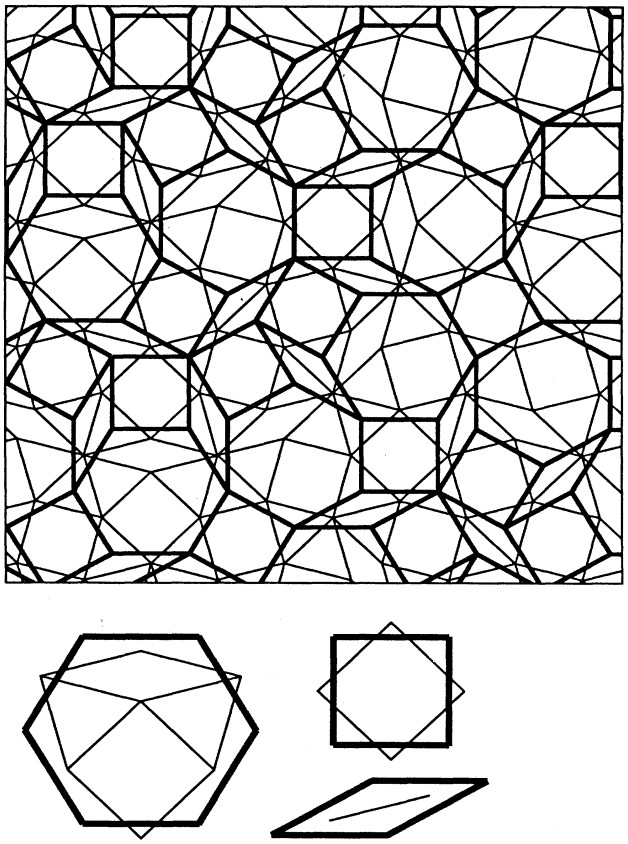

FIG. 17. The decoration of the PLI class tiling that produces the tiling proposed by Gähler as the basis of an atomic model of the dodecagonal phase of Ni-Cr.

The application of analytical techniques developed for the Penrose tilings to the cases of octagonal and dodecagonal symmetry has yielded rather remarkable results. The same basic techniques for construction and description of PLI class tilings have proven to be relevant in all three cases, and even the details of the analysis are quite similar. In light of the high degree of similarity, however, the slight differences take on added importance. Table IV lists the points of difference among the various symmetries of interest. The results for the icosahedral case are taken from the literature.[1] [Note, however, that the relation between the duals to the Ammann quasilattices (which consist of grids of planes normal to the vertex vectors of the icosahedron) and the tilings obtained by projection is not straightforward in this case and has yet to be fully characterized.]

The relationships among the different rows of Table IV are intriguing. Two issues that may be relevant to the analysis of icosahedral quasicrystals are the following. First, one of the mysteries central to the development of reliable theories of quasicrystal formation and structure is the connection between the parameters that arise in the analysis of discrete tiling models and those of canonical elasticity theory. Is it merely a coincidence that, for the 2D symmetries, the number of Ammann quasilattices required to enforce matching rules is the same as the number of elastic constants associated with phason fluctuations of finite wave vector? What should be expected for the icosahedral case? Second, as mentioned above, the possibility of producing a large, well-ordered quasicrystal may ultimately depend on the existence of a physically plausible growth algorithm that avoids the introduction of phason strain. Such an algorithm has been discovered for the Penrose tilings,[9] but it remains to be seen whether similar algorithms exist for other symmetries. Is there a connection between the existence of a local growth algorithm and the degree of complexity required for matching rules, or the number of irreducible phason strains?

The proper understanding of the entries in Table IV and the relevance of the PLI class tilings to physical systems would represent a significant advance toward a unified theory of solids with any orientational symmetry. It is hoped that the explicit displaying of the PLI class

TABLE IV. Comparison of decagonal, octagonal, dodecagonal, and icosahedral symmetries. The entries in the first three columns are discussed in the text. The entries for the case of icosahedral symmetry are obtained from the literature.

	Decagonal (C_{10v})	Octagonal (C_{8v})	Dodecagonal (C_{12v})	Icosahedral (Y_h)
Scale factor for deflation	$(1+\sqrt{5})/2$	$1+\sqrt{2}$	$2+\sqrt{3}$	$(1+\sqrt{5})/2$
Dimension of E (projection hyperspace[a])	5	4	6	6
Dimensions of $E^{\perp},\bar{E},E^{LI}$	3,2,1	2,2,0	4,2,2	3,3,0
No. of Phason elastic constants for uniform strains[b]	2	3	3	2
No. of Phason elastic constants for finite wavelength fluctuations[b]	1	2	2	2
Phonon-phason coupling	yes	yes	no	yes
No. of Ammann quasilattices required to rule out periodicity	1	2	2	1
No. of Ammann quasilattices required to ensure quasiperiodicity	1	2	2	?
Local growth algorithm	yes	?	?	?

[a]The dimension listed is the minimal one for which the perp-space structure of the rhombic tilings consists of uniformly filled regions of the same density.

[b]The difference between the number of elastic constants for uniform strains and the number for fluctuations for the 2D cases is due to the fact that a particular linear combination of the phason strain invariants acts as a boundary term. (See Sec. V A.) For icosahedral symmetry, no such combination exists.

tilings and the treatment of their properties given in this paper will facilitate progress toward that goal.

ACKNOWLEDGMENTS

I wish to thank D. DiVicenzo, P. Steinhardt, and D. Nelson for helpful conversations and S. Langer for graciously providing me a version of TILER, his elegant computer program for growing tilings constrained by matching rules. This work was supported by National Science Foundation Grant No. DMR-85-14638 and by the Harvard Society of Fellows.

APPENDIX A: LOCALLY CONGRUENT AMMANN QUASILATTICES

We wish to derive the conditions under which two Ammann quasilattices, $\{\alpha_n,\beta_n\}$ and $\{\delta_n,\gamma_n\}$, are locally congruent. We begin by defining three types of *equivalence transformations* of α_n and β_n, which yield quasilattices that are identical up to overall translation.

For pure translations, we have

$$\alpha_n \rightarrow \alpha_n + \mathbf{u}\cdot\mathbf{e}_n \ . \tag{A1}$$

To see that this corresponds to a uniform translation of the Ammann quasilattice, we write

$$\begin{aligned} \mathbf{x}_{nN}\cdot\mathbf{e}_n &= S\left[N+\alpha_n+\mathbf{u}\cdot\mathbf{e}_n+\frac{1}{\sigma'}\left\lfloor\frac{N}{\sigma}+\beta_n\right\rfloor\right] \\ \Longrightarrow (\mathbf{x}_{nN}-S\mathbf{u})\cdot\mathbf{e}_n &= S\left[N+\alpha_n+\frac{1}{\sigma'}\left\lfloor\frac{N}{\sigma}+\beta_n\right\rfloor\right] . \end{aligned} \tag{A2}$$

For umklapps, we have

$$\alpha_n \rightarrow \alpha_n + p_n + \frac{1}{\sigma'}q_n, \quad \beta_n \rightarrow \alpha_n - q_n + \frac{1}{\sigma}p_n \ . \tag{A3}$$

An unklapp transformation re-indexes the lines in each individual grid, without affecting the actual positions of the lines at all. We have

$$\begin{aligned} \mathbf{x}_{nN}\cdot\mathbf{e}_n &\rightarrow S\left[N+\alpha_n+p_n+\frac{1}{\sigma'}q_n\right. \\ &\quad \left.+\frac{1}{\sigma'}\left\lfloor\frac{N}{\sigma}+\beta_n-q_n+\frac{1}{\sigma}p_n\right\rfloor\right] \\ &\rightarrow S\left[(N+p_n)+\alpha_n+\frac{1}{\sigma'}\left\lfloor\frac{N+p_n}{\sigma}+\beta_n\right\rfloor\right] \\ &\rightarrow \mathbf{x}_n(N+p_n)\cdot\mathbf{e}_n \ . \end{aligned} \tag{A4}$$

For β translations, we have

$$\beta_n \to \beta_n + \mathbf{z}\cdot\bar{\mathbf{e}}_n, \quad \text{for } \mathbf{z} = \begin{cases} \sqrt{2}\left[m_1+\frac{1}{\omega}m_2,\ m_3+\frac{1}{\omega}m_4\right] & \text{(eightfold)} \quad \text{(A5a)} \\ 2\left[m_1+\frac{1}{\xi}m_2,\ m_3+\frac{1}{\xi}m_4\right] & \text{(twelvefold)}, \quad \text{(A5b)} \end{cases}$$

where m_i is an integer. Though most vectors are not of the form of $\mathbf{z}$, the set of possible values of $\mathbf{z}$ is dense in the plane. It can be seen by direct computation that for $\mathbf{z}$ of this form, we have $\mathbf{z}\cdot\bar{\mathbf{e}}_n$ of the form $p_n + 1/\sigma q_n$. Furthermore, after applying an umklapp to restore β_n to its original value, we find that the change in α_n has the form of a pure translation, with

$$\mathbf{u} = \begin{cases} \sqrt{2}\left[m_2-\frac{1}{\omega}m_1,\ m_4-\frac{1}{\omega}m_3\right] & \text{(eightfold)} \quad \text{(A6a)} \\ 2\left[m_2+\frac{1}{\xi}m_1,\ m_4+\frac{1}{\xi}m_3\right] & \text{(twelvefold)}. \quad \text{(A6b)} \end{cases}$$

We can now show that $\{\alpha_n,\beta_n\}$ and $\{\delta_n,\gamma_n\}$ are locally congruent if and only if there exist integers p_n, q_n and *arbitrary* vectors $\mathbf{u}, \mathbf{w}$ such that

$$\Delta\alpha_n \equiv \alpha_n - \delta_n = \mathbf{u}\cdot\mathbf{e}_n + p_n + \frac{1}{\sigma'}q_n \quad \text{(A7a)}$$

$$\Delta\beta_n \equiv \beta_n - \gamma_n = \mathbf{w}\cdot\bar{\mathbf{e}}_n - q_n + \frac{1}{\sigma}p_n\ . \quad \text{(A7b)}$$

Let $\{\delta'_n,\gamma'_n\}$ be the result of successively applying a β translation with $\mathbf{z}=\mathbf{w}-\delta\mathbf{w}$, an umklapp, and a pure translation to $\{\delta_n,\gamma_n\}$. Note that $\{\delta'_n,\gamma'_n\}$ is equivalent to $\{\delta_n,\gamma_n\}$ and that $\mathbf{z}$ can be chosen arbitrarily close to $\mathbf{w}$, since the set of possible $\mathbf{z}$ is dense in the plane. An umklapp and pure translation can always be chosen such that

$$\begin{aligned} \alpha_n - \delta'_n &= 0\ , \\ \beta_n - \gamma'_n &= \delta\mathbf{w}\cdot\bar{\mathbf{e}}_n\ . \end{aligned} \quad \text{(A8)}$$

We choose $\mathbf{z}$ such that $|\delta\mathbf{w}\cdot\bar{\mathbf{e}}_n|$ is less than both $|\beta_n|$ and $|\gamma'_n|$ for all n. Since $\alpha_n=\delta'_n$, the $N=0$ lines of $\{\alpha_n,\beta_n\}$ and $\{\delta'_n,\gamma'_n\}$ coincide exactly. Now the difference between β_n and γ'_n affects only those lines in the quasilattice that correspond to an N for which $1/\sigma N+\beta_n$ and $1/\sigma N+\gamma'_n$ have different integer parts. For any given integer M, $\mathbf{z}$ can be chosen such that $\delta\mathbf{w}\cdot\bar{\mathbf{e}}_n$ is small enough that $1/\sigma N+\beta_n$ and $1/\sigma N+\gamma'_n$ have the same integer part for all $|N|<M$. This implies that for any given region of finite size in either quasilattice, an equivalence transformation of the other can be found such that the two coincide exactly in that region. The two quasilattices are therefore locally congruent. It is straightforward to confirm that translations, umklapps, and β translations are the only equivalence transformations on $\{\alpha_n,\beta_n\}$.

APPENDIX B: DERIVATION OF THE PLI CLASS VALUES OF α_n AND β_n

The essential property of the PLI class is that rescaled deflation of an Ammann quasilattice (by application of the rule of Fig. 8) produces an Ammann quasilattice that is locally congruent to the original. We wish, therefore, to derive the values of $\{\alpha_n,\beta_n\}$ having the property

$$\begin{aligned} \Delta\alpha_n &\equiv \alpha_n - \alpha_n^* = \mathbf{u}\cdot\mathbf{e}_n + p_n + \frac{1}{\sigma'}q_n\ , \\ \Delta\beta_n &\equiv \beta_n - \beta_n^* = \mathbf{v}\cdot\bar{\mathbf{e}}_n - q_n + \sigma' p_n\ , \end{aligned} \quad \text{(B1)}$$

where $\{\alpha_n^*,\beta_n^*\}$ is the rescaled deflation of $\{\alpha_n,\beta_n\}$, given by Eqs. (16) and (12).

Consider first the eightfold case. Substituting the expressions for α_n^* and β_n^* from Eqs. (16) and (12) into Eq. (B1), we find the condition

$$\alpha_n(1-\omega) - \lfloor\beta_n\rfloor + \frac{1}{2}\left[1+\frac{1}{\omega}\right] + \frac{|\beta_n^*|}{\omega} = \mathbf{u}\cdot\mathbf{e}_n + p_n + \frac{q_n}{\omega}\ , \quad \text{(B2a)}$$

$$\beta_n\left[1+\frac{1}{\omega}\right] - \frac{\beta_n}{\omega} = \mathbf{v}\cdot\bar{\mathbf{e}}_n - q_n + \frac{p_n}{\omega}\ , \quad \text{(B2b)}$$

or

$$\alpha_n = \mathbf{u}'\cdot\mathbf{e}_n + \frac{1}{2}\left[P_n + \frac{Q_n}{\omega}\right] + \frac{1}{2\omega}\ , \quad \text{(B3a)}$$

$$\beta_n = \mathbf{v}'\cdot\bar{\mathbf{e}}_n + \frac{1}{2}\left[-Q_n + \frac{P_n}{\omega}\right], \quad \text{(B3b)}$$

where we have defined $P_n \equiv -p_n - \lfloor\beta_n\rfloor - q_n$, $Q_n \equiv -p_n - \lfloor\beta_n\rfloor + q_n$, $\mathbf{u}' \equiv \mathbf{u}/(1-\omega)$, and $\mathbf{v}' \equiv \mathbf{v}/(\omega-1)$ and we have used the fact that $\lfloor\beta_n^*\rfloor = -1$ for any value of β_n. Note that Q_n is even if and only if P_n is even. Now if they are both even for all n, then Eqs. (B3) simply describes a class of solutions locally congruent to

$$\alpha_n = \frac{1}{2\omega}\ , \quad \text{(B4a)}$$

$$\beta_n = 0\ . \quad \text{(B4b)}$$

Furthermore, it is easy to verify that we get the same result even if one or more of the P_n's is odd. Suppose that P_0 is odd and all the other P_n's are even. Defining $\mathbf{u}''=\mathbf{u}'-(\frac{1}{2})(1+1/\omega,0)$ and $\mathbf{v}''=\mathbf{v}'-(\frac{1}{2})(-1+1/\omega,0)$ and substituting into Eqs. (B3), we get an equation of the identical form with $\mathbf{u}''$ replacing $\mathbf{u}'$, $\mathbf{v}''$ replacing $\mathbf{v}'$, and all the new values of P_n and Q_n even. Octagonal symmetry guarantees that similar manipulations can be performed for other values of n than 0 and it is clear that the different P_n's can be handled independently, since con-

verting one of them from even to odd does not affect the values of the others, modulo 2. We have thus demonstrated, for the eightfold case, that there is only one LI class of solutions to Eq. (B1) which must be the PLI class of Ammann quasilattices.

In the twelvefold case, an equation analogous to Eqs. (B3) is straightforward to obtain. We find

$$\alpha_n = \mathbf{u}' \cdot \mathbf{e}_n + \frac{1}{2}\left[P_n + \frac{Q_n}{\xi}\right] - \frac{1}{2\xi} , \tag{B5a}$$

$$\beta_n = \mathbf{v}' \cdot \bar{\mathbf{e}}_n + \frac{1}{2}\left[Q_n + \frac{P_n}{\xi}\right] , \tag{B5b}$$

where $P_n \equiv -p_n - \lfloor \beta_n \rfloor - 1 + q_n$, $Q_n \equiv p_n - \lfloor \beta_n \rfloor - 1 + 3q_n$. Once again P_n and Q_n are either both even or both odd. Unlike in the eightfold case, however, if P_n is odd for certain values of n, it is not possible to absorb all of the half-integral terms in Eqs. (B5) into $\mathbf{u}$ and $\mathbf{v}$, as was done in the eightfold case. We state without proof that there are four distinct LI classes that solve the equation: the LI class corresponding to P_n even for all n, the one corresponding to P_n odd for all n, the one corresponding to P_n even for $n = 0,2,4$ only, and the one corresponding to P_n even for $n = 1,3,5$ only. (All other possibilities are locally congruent to one of these.) Of these, only the first two have dodecagonal symmetry; the others have only hexagonal symmetry, as can be seen most easily by inspection of the tilings dual to the Ammann quasilattices. Inspection of an Ammann quasilattice in each of the first two LI classes immediately reveals that the PLI class corresponds to P_n even for all n, as asserted in Eq. (5).

[1] P. J. Steinhardt and S. Ostlund, *The Physics of Quasicrystals* (World Scientific, Singapore, 1987).
[2] C. L. Henley, Comments Cond. Matter Phys. **13**, 59 (1987).
[3] L. S. Levitov Zh. Eksp. Teor. Fiz. **93**, 1832 (1987) [Sov. Phys.—JETP **66**, 1046 (1987)].
[4] R. Penrose, Bull. Inst. Math. Appl. **10**, 266 (1974).
[5] J. E. S. Socolar and P. J. Steinhardt, Phys. Rev. B **34**, 617 (1986).
[6] D. Levine and P. J. Steinhardt, Phys. Rev. B **34**, 596 (1986).
[7] M. Gardner, Sci. Am. **236**, 110 (1977).
[8] A. Garg and D. Levine, Phys. Rev. Lett. **59**, 1683 (1987).
[9] G. Y. Onoda, P. J. Steinhardt, D. P. DiVincenzo, and J. E. S. Socolar, Phys. Rev. Lett. **60**, 2653 (1988).
[10] N. de Bruijn, Proc. K. Ned. Akad. Wet., Ser. A **84**, 39 (1981).
[11] B. Grunbaum and G. C. Shephard, *Tilings and Patterns* (Freeman, San Francicso, 1986).
[12] R. Ammann (private communication).
[13] D. M. Frenkel, C. L. Henley, and E. D. Siggia, Phys. Rev. B **34**, 3649 (1986).
[14] P. Stampfli, Helv. Phys. Acta **59**, 1260 (1986).
[15] N. Niizeki and H. Mitani, J. Phys. A **20**, L405 (1987).
[16] J. E. S. Socolar, Ph.D. thesis, University of Pennsylvania, 1987.
[17] M. Duneau and A. Katz, Phys. Rev. Lett. **54**, 2688 (1985).
[18] J. E. S. Socolar, T. C. Lubensky, and P. J. Steinhardt, Phys. Rev. B **34**, 3345 (1986).
[19] D. Levine and P. J. Steinhardt, Phys. Rev. Lett. **53**, 2477 (1984).
[20] V. Elser, Acta Crystallogr. Sect. A **42**, 36 (1986).
[21] D. Levine, T. C. Lubensky, S. Ostlund, S. Ramaswamy, P. J. Steinhardt, and J. Toner, Phys. Rev. Lett. **54**, 1520 (1985).
[22] J. E. S. Socolar, D. Levine, and P. J. Steinhardt, Phys. Rev. B **32**, 5547 (1985).
[23] F. Gahler and J. Rhyner, J. Phys. A **19**, 267 (1986).
[24] N. de Bruijn, Proc. K. Ned. Akad. Wet., Ser. A **84**, 27 (1981).
[25] The tedium of this task was greatly reduced with the aid of a computer program written by S. Langer for adding forced tiles to an arbitrary cluster.
[26] P. Bak, Phys. Rev. B **32**, 5764 (1985).
[27] M. Tinkham, *Group Theory and Quantum Mechanics* (McGraw-Hill, New York, 1964).
[28] P. A. Kalugin, A. Kitaev, and L. S. Levitov, J. Phys. (Paris) Lett. **46**, L601 (1985).
[29] C. L. Henley, J. Phys. A **21**, 1649 (1988).
[30] P. De and R. A. Pelcovits, Phys. Rev. B **35**, 5774 (1987).
[31] M. Jarić, private communication.
[32] T. C. Lubensky, S. Ramaswamy, and J. Toner, Phys. Rev. B **32**, 7444 (1985).
[33] F. Gahler, in *Quasicrysalline Materials,* edited by C. Janot and J. M. Dubois (World Scientific, Singapore, in press).